ORIGINAL RESEARCH

Inhibition of Senescence-Associated Genes *Rb1* and *Meis2* in Adult Cardiomyocytes Results in Cell Cycle Reentry and Cardiac Repair Post–Myocardial Infarction

Perwez Alam, PhD; Bereket Haile, BS; Mohammed Arif, PhD; Raghav Pandey, PhD; Miso Rokvic, BS; Michelle Nieman, BS; Bryan D. Maliken, PhD; Arghya Paul, PhD; Yi-Gang Wang, PhD; Sakthivel Sadayappan, PhD; Rafeeq P. H. Ahmed, PhD; Onur Kanisicak, PhD

***Background*—**Myocardial infarction results in a large-scale cardiomyocyte loss and heart failure due to subsequent pathological remodeling. Whereas zebrafish and neonatal mice have evident cardiomyocyte expansion following injury, adult mammalian cardiomyocytes are principally nonproliferative. Despite historical presumptions of stem cell–mediated cardiac regeneration, numerous recent studies using advanced lineage-tracing methods demonstrated that the only source of cardiomyocyte renewal originates from the extant myocardium; thus, the augmented proliferation of preexisting adult cardiomyocytes remains a leading therapeutic approach toward cardiac regeneration. In the present study we investigate the significance of suppressing cell cycle inhibitors *Rb1* and *Meis2* to promote adult cardiomyocyte reentry to the cell cycle.

***Methods and Results*—**In vitro experiments with small interfering RNA–mediated simultaneous knockdown of *Rb1* and *Meis2* in both adult rat cardiomyocytes, isolated from 12-week-old Fischer rats, and human induced pluripotent stem cell–derived cardiomyocytes showed a significant increase in cell number, a decrease in cell size, and an increase in mononucleated cardiomyocytes. In vivo, a hydrogel-based delivery method for small interfering RNA–mediated silencing of *Rb1* and *Meis2* is utilized following myocardial infarction. Immunofluorescent imaging analysis revealed a significant increase in proliferation markers 5-ethynyl-2′-deoxyuridine, PH3, KI67, and Aurora B in adult cardiomyocytes as well as improved cell survivability with the additional benefit of enhanced peri-infarct angiogenesis. Together, this intervention resulted in a reduced infarct size and improved cardiac function post–myocardial infarction.

***Conclusions*—**Silencing of senescence-inducing pathways in adult cardiomyocytes via inhibition of *Rb1* and *Meis2* results in marked cardiomyocyte proliferation and increased protection of cardiac function in the setting of ischemic injury. **(*J Am Heart Assoc*. 2019;8:e012089. DOI: 10.1161/JAHA.119.012089.)**

Key Words: adult cardiomyocytes • angiogenesis • cardioprotection • cardiovascular disease • induced cell cycle reentry • microRNA • myocardial infarction

The massive loss of adult cardiomyocytes (ACMs) is the leading cause of heart failure after myocardial ischemic injury, resulting in the replacement of cardiac tissue with a nonfunctional scar, restricting cardiac output and heart function.[1] Although there has been extensive research effort in the field of regenerative medicine to repair the infarcted myocardium, the challenge of replenishing lost cardiomyocytes has persisted to this date with limited success, and many previously promising avenues that led to clinical trials are now deemed ineffective.[2] For example, nearly 20 years of research aimed at harnessing the alleged endogenous regenerative potential of mammalian heart by generating de novo cardiomyocytes from an elusive resident cardiac stem cell population appears to have now been

From the Department of Pathology and Laboratory Medicine, College of Medicine (P.A., B.H., M.A., R.P., M.R., B.D.M., Y.-G.W., R.P.H.A., O.K.), Department of Molecular and Cellular Physiology, College of Medicine (M.N.), and Department of Internal Medicine, Heart, Lung and Vascular Institute (S.S.), University of Cincinnati, OH; BioIntel Research Laboratory, Department of Chemical and Petroleum Engineering, Bioengineering Graduate Program, School of Engineering, University of Kansas, Lawrence, KS (A.P.).

Accompanying Tables S1 through S6, Figures S1 through S19, and Video S1 are available at https://www.ahajournals.org/doi/suppl/10.1161/JAHA.119.012089

Correspondence to: Onur Kanisicak, PhD, or Perwez Alam, PhD, 231 Albert Sabin Way, Cincinnati, OH 45267. E-mails: onur.kanisicak@uc.edu, alampz@ucmail.uc.edu

Received March 1, 2019; accepted May 31, 2019.

Clinical Perspective

What Is New?

- This is the first study to show the clinical potential of hydrogel-based delivery of small interfering RNAs to knock down cell cycle inhibitors *Rb1* and *Meis2*, which effectively prevents cell death, induces cardiomyocyte reentry to the cell cycle, and stimulates secretion of proangiogenic cardiokines.
- In vivo studies showed improved cardioprotection with a decreased infarct size and improved cardiac function in comparison to control.
- Our study reveals that the enhanced peri-infarct angiogenesis is stimulated directly by cytokines secreted from cycling small interfering RNA transfected cardiomyocytes.

What Are the Clinical Implications?

- The senescent nature of adult mammalian cardiomyocytes is a major limiting factor that prevents regeneration resulting in heart failure.
- Our study demonstrates that the simultaneous inhibition of *Rb1* and *Meis2* could be a novel and potential therapeutic intervention to improve cardiac repair, and function post–myocardial infarction.
- The hydrogel-based in vivo delivery of small interfering RNAs utilized in this study shows promising results for applications with a gene-silencing approach, especially highlighting the site-specific, sustained gene repression as an effective and potential therapeutic method.

debunked with accruing evidence, not only showing lack of endogenous regeneration from stem cells but no cardiomyocyte replacement from any noncardiomyocyte source.[3,4] Mammalian ACMs are terminally differentiated cells with minimal endogenous proliferative capacity following myocardial infarction (MI),[5] whereas several lower organisms such as zebrafish, newts, and even neonatal mice can regenerate damaged myocardium through the proliferation of preexisting cardiomyocytes.[6-8] Therefore, the development of novel therapeutic interventions to regenerate ischemic myocardium by inducing proliferation of preexisting ACMs has become an even more critical area of research.[9-12] A significant limitation on cardiomyocyte proliferation stems from ACMs acquiring a senescent phenotype during postnatal development with extensive cellular remodeling followed by elevated gene expression levels of cell cycle inhibitors (*Rb1, p16, p53, IL6*).[13-16] Therefore, senescent ACMs are presumed unable to proliferate during physiological or disease conditions, even though experimental external stimuli such as hypoxia or microRNA overexpression have been shown to trigger ACMs to reenter the cell cycle.[12,17-19]

In our recent publication we identified miR-1825 as a proliferation-inducing microRNA with *Retinoblastoma1* (*Rb1*) and *Meis* homeobox 2 (*Meis2*) as its downstream targets of inhibition. In the heart these cell cycle inhibitors have a gene expression pattern restricted to postnatal development[20-23] during which upregulation of *Rb1* leads to oxidative phosphorylation and associates with prosenescent phenotypic changes.[21,24] Briefly, unphosphorylated *Rb1* acts as a negative regulator of the cell cycle by binding and inhibiting the E2F family transcription factors, which restrict cell cycle progression at G_1-S phase.[23,25] On phosphorylation, *Rb1* becomes inactive and allows E2F-driven cell cycle progression,[26,27] while also acting through the downregulation of cell cycle inhibitors p21Waf1/Cip1 and p27Kip1.[28] Moreover, *Rb1*-mediated E2F activity can control cell proliferation beyond cell cycle regulation by inducing DNA synthesis and blocking apoptosis through p53-dependent/independent pathways.[29,30] Similarly, *Meis2* acts as a transcription regulator of the differentiated state in which high levels of MEIS expression are associated with reduced proliferation, increased cell-cell adhesion, and a more mature differentiated state.[31] On the other hand, inhibition of *Meis2* expression leads to decreased expression of *p15*, a cell cycle inhibitor, and thereby supports cell cycle progression.[32]

These findings suggest that the *Rb1/Meis2*-mediated cell cycle arrest may have a central role in the senescent phenotype of adult cardiomyocytes for which we hypothesized that simultaneous inhibition of *Rb1* and *Meis2* would lead to cell cycle reentry of adult cardiomyocytes and promote cardiac repair post-MI. Here we show that, with small interfering (si)RNA-based repression of *Rb1* and *Meis2*, we can sufficiently induce proliferation of adult rat cardiomyocytes and human induced pluripotent stem cell–derived cardiomyocytes (hiPSc-CMs). Furthermore, we have observed a cardiomyocyte-mediated proangiogenic stimulation of endothelial cells through cytokine secretion from proliferating cardiomyocytes, together resulting in improved wound healing and cardioprotection against ischemia-induced heart failure in vivo.

Methods

Data Availability

The authors declare that all supporting data are available within the article and its online supplementary files. For purposes of reproducibility, additional technical information and data that support the findings of this study are available from the corresponding authors on reasonable request.

Animal Studies

Young 12-week-old male Fischer-344 rats (n=42) acquired from Charles River (Wilmington, MA) were used in this study.

All experiments in this study involving rats were approved by the Institutional Animal Care and Use Committee at the University of Cincinnati.

Isolation and Culture of ACM

ACMs were isolated from 12-week-old Fischer rats using the standard Langendorff procedure as described previously.[11,33] Briefly, we dissected rat hearts and perfused with Krebs-Henseleit bicarbonate buffer, followed by perfusion with digestion buffer E until the heart became flaccid. Next, we transferred the heart from the Langendorff apparatus to a sterile laminar flow hood where we performed the remaining portion of the procedure. We dissected the atria from the heart, and the remaining ventricular tissue was then minced in digestion buffer. This cell suspension was then filtered through a 100-μm cell strainer (BD Biosciences, Franklin Lakes, NJ) followed by centrifugation at 20*g* for 3 minutes. The supernatant was discarded, and cells were resuspended in 25 mL of buffer B and allowed to settle down via gravity. The procedure was repeated with 25 mL of fresh buffer B. Isolated ACMs were then cultured in DMEM (GE Healthcare, Little Chalfont, UK) supplemented with 10% fetal bovine serum (FBS) (Fisher Scientific, Waltham, MA) and 5 mmol/L penicillin/streptomycin (Fisher Scientific), at 37°C in a 5% CO_2 incubator for 24 hours before transfection. Compositions of all the solutions are provided in Table S1.

Transfection of ACM

siRNAs against *Rb1* and *Meis2* were used in an equimolar combination (50 nmol/L each), designated as "siRNA-cocktail" to simultaneously inhibit *Rb1* and *Meis2*. ACMs were transfected 24 hours after isolation using Lipofectamine RNAiMAX (Thermo Fisher Scientific, Waltham, MA) according to the manufacturer's protocol. *Caenorhabditis elegans*-miR-67 (*Cel*-miR-67) (Dharmacon, Lafayette, CO) was used as the transfection control. We used *Cel*-miR-67 as scrambled control for all experiments[34,35] because it has minimal sequence identity with microRNAs present in human, mouse, and rat and has the same design and modifications as the other siRNAs. *Cel*-miR-67 has been widely utilized as a scrambled control in cardiovascular studies and shown to have no cardioprotective effect either in vitro in isolated cardiomyocytes or in vivo experiments after cardiac injury.[34-36] In this and our previous studies we also conducted extensive optimization experiments with control groups such as "no transfection" along with "*Cel*-miR-67 scrambled transfection" using both cardiomyocytes and noncardiomyocyte cell populations and showed no change in cell morphology, proliferation rate, viability, or gene expression (data not shown).[34,35] Therefore, *Cel*-miR-67 scrambled control is used as the standard negative control for all of our in vitro experiments. All siRNAs variants were procured from Ambion, Thermo Fisher Scientific (Waltham, MA). Cells were cultured for 7 days. Every 24 hours following transfection, the medium was refreshed with culture medium containing 0.5% of 5-ethynyl-2′-deoxyuridine (EdU) (Life Technologies, Carlsbad, CA). Posttransfection assays were performed on day 7 after transfection.[11,34] Transfection efficiency was determined using the siRNAs labeled with cy547 and siUbC as previously described.[37] Sequences for siRNAs are provided in Table S2. The specificity of siRNAs was analyzed through sequence homology analysis. We observed a significant homology for siRb1 and siMeis2, only with *Rb1* (Figure S18 and Table S3) and *Meis2* (Figure S19 and Table S4) genes, respectively. Immunocytochemical and molecular analyses were performed on day 7 after transfection.

Immunocytochemistry

On day 7, cardiomyocytes were fixed with 4% (w/v) paraformaldehyde, followed by permeabilization with 0.1% Triton X-100 for 15 minutes at room temperature. Cells were then washed 3 times with PBS and blocked with CAS-Block (Life Technologies, Carlsbad, CA) for 1 hour at room temperature. Next, cells were incubated overnight at 4°C with specific primary antibodies (1:200 diluted) in CAS-Block. Following this, cells were washed 3 times with PBS and incubated for 1 hour at room temperature with a fluorophore-linked secondary antibody diluted (1:200) in CAS-Block. The nucleus was then stained with 4′,6-diamidino-2-phenylindole (DAPI) through a 20-minute incubation at room temperature. A cardiac-specific marker, Troponin I (TnI), was used to stain ACMs. In addition, we also used a nuclear cardiac-specific marker, NKx2.5, for validation. The images were taken using a fluorescence microscope (Olympus) at various magnifications. Details of the antibodies used are provided in Table S5.

ACM Proliferation

To evaluate ACM proliferation we used specific markers to track different stages of the cell cycle. DNA synthesis was detected through EdU staining by culturing ACMs in 5 μmol/L of an EdU (a nucleoside analogue of thymidine)-supplemented medium, which results in EdU incorporation into newly synthesized DNA strands. EdU incorporation was visualized by Click-iT EdU labeling kit (Invitrogen, Carlsbad, CA) according to the manufacturer's protocol. Moreover, the synthesis, mitosis, and cytokinesis phases of proliferation were identified by immunostaining for KI67, PH3, and Aurora B, respectively, as described earlier.[35,37] In addition to proliferation markers, ACMs were stained for the cardiac-specific

marker TnI and scored for dual-positive ACMs to quantify the proliferation rate. All of the experiments were performed in triplicate.

Human Induced Pluripotent Stem Cell–Derived Cardiomyocyte Proliferation

We used hiPSc-CMs to evaluate the siRNA-cocktail-mediated proliferation in human cardiomyocytes. The hiPSc-CMs were procured from Cellular Dynamics International (Madison, WI) and cultured in iCell cardiomyocyte maintenance medium (Cellular Dynamics International) as per the manufacturer's protocol. Transfection of hiPSc-CMs with siRNA-cocktail and the quantification of the proliferation rate were performed as described above but with the analyses performed on day 5 posttransfection instead of day 7 for rat ACMs.

ACM Survival

To evaluate the ACM survival rate, we measured apoptosis in both the siRNA-cocktail and *Cel*-miR-67–transfected groups using terminal deoxynucleotidyl transferase dUTP nick end labeling (TUNEL) assay (Roche, Switzerland). ACMs were fixed and permeabilized, and apoptosis was measured through TUNEL assay per the manufacturer's protocol. All the experiments were performed in triplicate.

RNA Extraction and cDNA Synthesis

Total RNA was isolated using trizol reagent (Thermo Fisher Scientific, Waltham, MA) per the standard protocol. In brief, ACMs were harvested on day 7 after transfection and washed twice with PBS. Cells were suspended in 1 mL of trizol reagent and pipetted several times to homogenize. Likewise, the heart tissue homogenate was prepared in 1 mL of trizol reagent. The solution was kept at room temperature for 5 minutes, and then 0.2 mL of chloroform per 1 mL of trizol was added, which was followed by 2 to 3 minutes of incubation at room temperature and centrifugation at 12 000*g* for 20 minutes at 4°C. The resulting aqueous phase was separated out into a new tube, and RNA was precipitated by adding 0.5 mL of isopropanol. The precipitate was incubated for 10 minutes at room temperature and centrifuged at 12 000*g* for 20 minutes at 4°C. The supernatant was discarded, and the pellet was washed with 1 mL of 75% ethanol and air dried for 10 to 15 minutes. The pellet was dissolved in 30 to 50 μL of Tris 10 mmol/L + EDTA 1 mmol/L), and RNA concentration was measured by a NanoVue Plus Spectrophotometer (GE Healthcare, Little Chalfont, UK). cDNA synthesis was performed with 1 μg of total RNA, using Omniscript Reverse Transcription kit (QIAGEN, Germantown, MD) per the manufacturer's protocol.

Real-Time PCR

Real-time polymerase chain reaction (RT-PCR) was performed by using specific primer pairs for respective genes as listed in Table S6. RT-PCR primers were synthesized using Primer3web version 4.0.0 (http://bioinfo.ut.ee/primer3/). Amplification reactions were performed in triplicate in CFX Connect Real-Time PCR Detection System (Bio-Rad, Hercules, CA) by using Applied Biosystems SYBR Green PCR Master Mix (Thermo Fisher Scientific, Waltham, MA). Quantification of RT-PCR was performed by the ΔΔCt method with β-actin serving as the control.

Western Blot

For Western blotting, the total protein was isolated using a radioimmunoprecipitation assay buffer (Thermo Fisher Scientific, Waltham, MA), following the standard protocol. Protein from neonatal rat cardiomyocytes was isolated from 24- to 48-hour-old rat hearts, whereas ACM protein was isolated from 12-week-old rat hearts. Heart tissue homogenates were prepared in radioimmunoprecipitation assay buffer, and digestion was performed through a 1-hour incubation on a rocking shaker at 4°C. Lysates were centrifuged at 12450*g* for 15 minutes at 4°C, and the supernatant was collected in fresh tubes. Protein concentration was estimated by the bicinchoninic acid method, using a bicinchoninic acid protein assay kit (Sigma Aldrich, St. Louis, MO). Fifty micrograms of protein was separated on 10% SDS-PAGE gel and transferred to a polyvinylidene fluoride membrane. Blocking was performed by incubating the membrane with 5% skimmed milk in Tris-buffered saline with Tween 20 for 1 hour at room temperature. Proteins of interest were detected by overnight incubation of membranes with specific primary antibodies (diluted in 5% skimmed milk in Tris-buffered saline with Tween 20) at 4°C, followed by a 1-hour incubation with horseradish peroxidase–conjugated secondary antibody at room temperature. Protein bands were visualized by treating the membrane with Super Signal W Femto Maximum Sensitivity Enhanced Chemiluminescence (Thermo Fisher, Waltham, MA) and developed onto a chemiluminescence film.

Preparation of Hydrogel With siRNA-Cocktail

We utilized a nanocomposite hydrogel to deliver siRNA-cocktail in the infarcted adult rat heart. We obtained the injectable nanocomposite hydrogels from our collaborator, Dr Arghya Paul at the University of Kansas (Lawrence, KS).[38] The hydrogel had been previously characterized for the advantage of controlled and site-specific cardiac drug delivery.[38-40] A lipid emulsion of siRNAs was prepared by mixing siRNAs with MaxSuppressor In Vivo RNA-LANCEr II (PerkinElmer, Waltham, MA) reagent, by following the manufacturer's protocol. In brief, we mixed equal amounts of siRb1 and siMeis2 with

MaxSuppressor In Vivo RNA-LANCEr II reagent followed by a 5-minute sonication on a high power setting. Next, equal volumes of lipid emulsion siRNA-cocktail and nanocomposite hydrogel were mixed to prepare the final siRNA complex for intramyocardial injection. We used 12-week-old rats and divided our animals into 3 study groups: (1) no treatment: LAD ligation without any treatment (N=6); (2) hydrogel: LAD ligation and 100 μL of nanocomposite hydrogel, which was injected at multiple sites in the infarcted area (N=6); (3) hydrogel+siRNA-cocktail: LAD ligation and 100 μL of nanocomposite hydrogel infused with siRNA-cocktail was injected at various locations in the infarcted area (N=6). The animals were maintained on buprinex after surgery for 24 hours. For heart function studies, transthoracic echocardiography was performed at day 3 and day 21 after surgery, and subsequently, animals were euthanized, and their hearts were harvested for molecular and histological analyses.

Myocardial Infarction

A model of myocardial infarction was used in adult (12-week-old) male Fischer 344 rats by left anterior descending coronary artery (LAD) ligation. Animals were anesthetized with isoflurane gas followed by tracheal intubation and ventilation using a rodent ventilator (Minivent, Type 845, Hugo Sachs Elektronik, March-Hugstetten, Germany). Animal body temperature was maintained at 37°C during the surgery. Hearts were exposed by minimal left-sided thoracotomy. Myocardial infarction was created by ligation with permanent occlusion of the LAD, per our standardized protocol.[35,37,38] After LAD ligation, 100 μL of nanocomposite biocompatible hydrogel (5.0% [w/v] gelatin, 2.0% [w/v] silicate nanoparticles, dissolved in PBS) or hydrogel with siRNA-cocktail were intramyocardially injected at multiple sites in the infarcted area (3-4 sites/heart on average).[38]

In Vivo Assessment of Cardiac Function

Cardiac function was assessed by transthoracic echocardiography on day 3 and day 21 after surgery, using a Vevo 2100 Imaging System (VisualSonics, Toronto, Canada) with a 24-MHz transducer, MS250. Animals were anesthetized with isoflurane gas, and 2-dimensional imaging of their hearts was performed and recorded for M-mode through the anterior and posterior left ventricle (LV) walls. Anterior and posterior wall thickness (end-diastolic and end-systolic) and LV internal dimensions were measured from at least 3 consecutive cardiac cycles. Indices of the LV systolic function, including LV ejection fraction and cardiac output, were calculated as LVejection fraction (%)=[(LV end-diastolic dimension)^3−(LV end-systolic dimension)^3/(LV end-diastolic dimension)^3]×100; cardiac output=heart rate×stroke volume. Furthermore, a speckle tracking–based, detailed wall function analysis was performed by VevoStrain analysis tool (VisualSonics, Toronto, Canada). Images acquired from long-axis echoes were used to analyze the radial strain, radial strain rate, radial displacement, and radial velocity. Six myocardial wall segments were imaged: posterior basal, posterior middle, posterior apex, anterior basal, anterior middle, and anterior apex. Of these, the anterior middle, anterior apex, and posterior apex segments were considered as the area under infarct, and, thus, the average of these segments was used for the aforementioned myocardial deformation analysis (Figure S16A and S16B).

In Vivo Experiments, Anesthesia, and Euthanasia

All experimental procedures performed on rodents followed National Institutes of Health guidelines and protocols approved by the Institutional Animal Care and Use Committee at the University of Cincinnati. The experimental rats were maintained and housed under specific, pathogen-free conditions established by the Laboratory Animal Medical Services at the University of Cincinnati. All the experiments were performed in a dedicated procedure room approved by the Institutional Animal Care and Use Committee for performing animal surgeries. We followed the Institutional Animal Care and Use Committee and Laboratory Animal Medical Services approved guidelines for euthanasia. We anesthetized the rats by administering 100% O_2 with 4% isoflurane. The animals were maintained under anesthesia by continuous administration of 100% O_2 together with 2.5% isoflurane throughout the surgery. After 21 days following surgery, we euthanized the rats by an overdose of sodium pentobarbital followed by thoracotomy to isolate the hearts.

Histological Examination and Immunohistochemistry

For immunostaining, paraffin-embedded heart sections were deparaffinized first by xylene, followed by 100%, 90%, and 80% ethanol washes (5 minutes each). For antigen retrieval, we heated the slides in a pressure cooker for 3 minutes in 0.1 mol/L citrate buffer (pH 6.0) followed by cooling for 45 minutes. Heart sections were then blocked with CAS-block (Thermo Fisher Scientific, Waltham, MA) for 1 hour at room temperature followed by 3 PBS washes for 5 minutes each. Primary antibodies were used in a working dilution of 1:200 with CAS-Block and were individually incubated overnight at 4°C followed by 3 PBS washes for 5 minutes each. The corresponding fluorophore-linked secondary antibodies linked with Alexa Fluor (Thermo Fisher, Waltham, MA) were used in a working dilution of 1:200 with CAS-Block and were incubated for 2 hours at room temperature, followed by 3 PBS washes for 5 minutes each. The nucleus was stained with DAPI (Sigma-Aldrich, St. Louis, MO). We used fluorescence and confocal microscopes to visualize and capture the images.

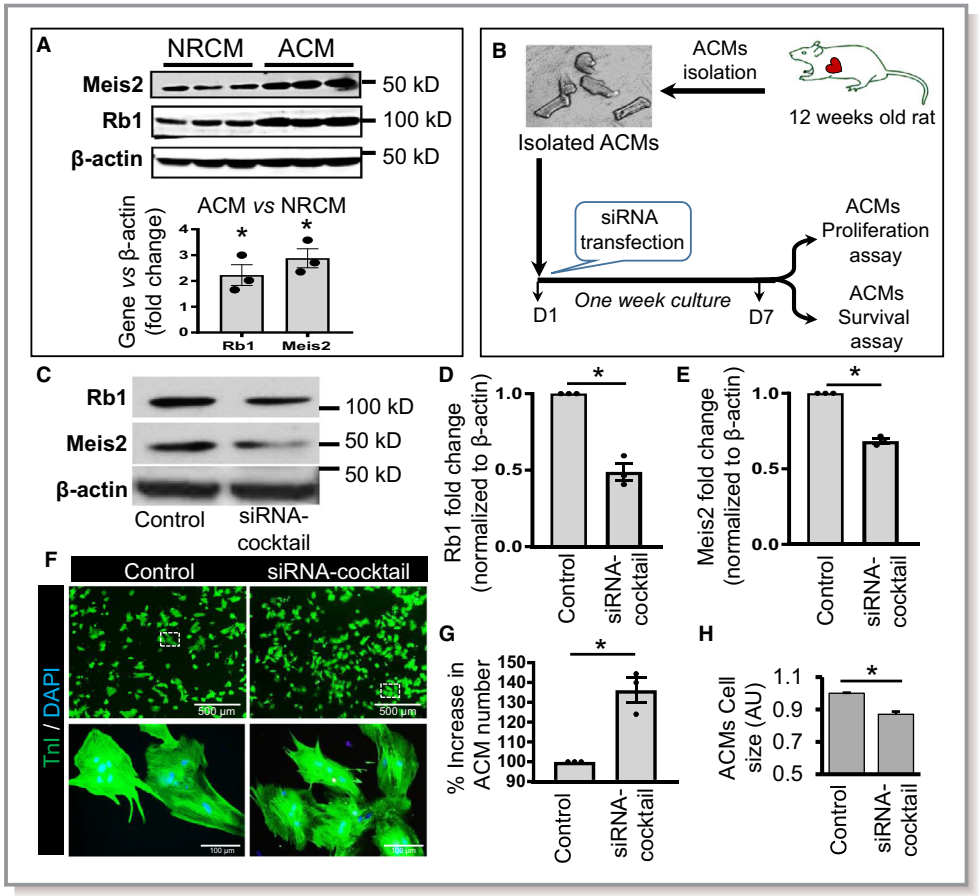

Figure 1. Simultaneous inhibition of *Rb1* and *Meis2* leads to ACM proliferation. **A**, The expression analysis of Rb1 and Meis2 was performed through Western blot showing a significant increase in the expression of Rb1 and Meis2 in ACM when compared with NRCM. N=3 rats per group. **B**, Schematic representation of in vitro experimental design, illustrating ACM isolation, transfection with *Cel*-miR-67 (control) and siRNA-cocktail on day 1, followed by ACM proliferation and survival assays on day 7. **C**, Representative immunoblots for Rb1 and Meis2. Immunoblotting was performed with cell lysate from ACMs, transfected with siRNA-cocktail and control. **D** and **E**, Densitometric analysis showed regulation in the expression of cell cycle regulators in the siRNA-cocktail–transfected group in comparison to control. **F** and **G**, Representative immunostained images of ACMs showing an increase in cell number in the siRNA-cocktail–transfected group on day 7 after transfection vs control. **H**, Quantification of ACM size shows a significant decrease in ACM size in the siRNA-cocktail–transfected group vs control. Immunostaining shows a significant increase in (**I** and **J**) EdU-positive ACMs, (**K** and **L**) KI67-positive ACMs, (**M** and **N**) PH3-positive ACMs, and (**O** and **P**) Aurora B–positive ACMs in siRNA-cocktail–transfected groups vs control. We used ACMs, isolated from adult rats (≈12 weeks old) for all in vitro experiments. N=3 rats, n=8 experimental replicates each, and n=3 images each. Scale bar=100 μm or as cited in the image. Panels in White rectangles represent respective enlarged sections. Yellow arrows indicate the ACMs labeled with the indicated proliferative markers. ACM indicates adult cardiomyocyte; DAPI, 4′,6-diamidino-2-phenylindole; EdU, 5-ethynyl-2′-deoxyuridine; NRCM, neonatal rat cardiomyocyte; PH3, phosphor histone 3; siRNA, short interfering RNA; TnI, Troponin I. Results are presented as mean±SEM; *$P \leq 0.05$. $P \leq 0.05$ was considered statistically significant.

Tube Formation Assay

To perform the endothelial tube formation assay, human umbilical vein endothelial cells (HUVECs) were cultured with conditioned medium from ACMs transfected with siRNA-cocktail (CMe-siRNA-cocktail) or *Cel*-miR-67 (CMe-control) on matrigel (Geltrex Reduced Growth Factor Basement Membrane Matrix, Invitrogen, Carlsbad, CA). Then, 48-well culture plates were precoated with 50 μL of Matrigel/well and incubated at 37°C for 30 minutes. HUVECs were seeded at a density of 42 000 cells/cm^2 in each well of a 48-well plate. Endothelial tube formation study was performed in 3 groups: (1) control: HUVECs were seeded with conditioned medium, collected from *Cel*-miR-67–transfected ACMs; (2) CMe-siRNA-cocktail: HUVECs were

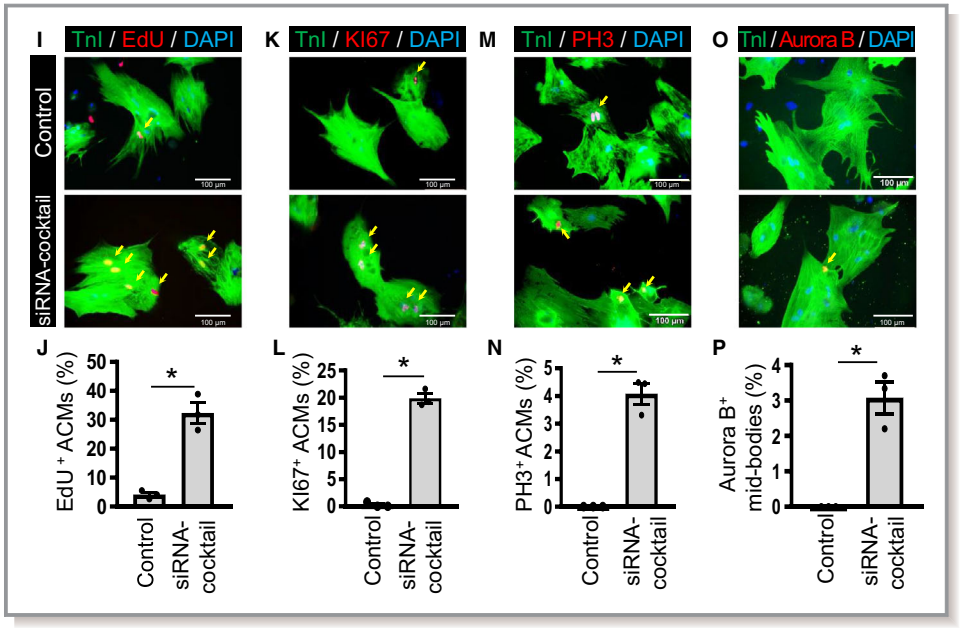

Figure 1. Continued.

seeded with conditioned medium collected from ACMs transfected with *Rb1*/*Meis2* siRNA-cocktail; and (3) positive control: HUVECs were seeded with serum-free endothelial medium supplemented with vascular endothelial growth factor (30 ng/mL media). HUVECs were cultured for 8 hours before analysis. Analysis of endothelial tube formation assay for total tube length and branching points was performed by Wimasis (2017) image analysis tool (WimTube: Tube Formation Assay Image Analysis Solution, Release 4.0; Onimagin Technologies, Córdoba, Spain). At least 3 images from each group were analyzed for endothelial tube formation assay.

Statistical Analyses

All reported values are expressed as mean±standard error of the mean. We used GraphPad Prism 8 software (GraphPad, San Diego, CA) to evaluate the validity of our sample size and the normal distribution using the Shapiro-Wilk test for each experimental group when comparing only 2 groups. Normally distributed data were analyzed using a 2-way, unpaired t test. A value of $P<0.05$ was considered statistically significant. Additionally, we performed a 1-way ANOVA with Tukey HSD post hoc analysis to calculate the statistical significance among the groups for in vivo studies.

Results

In Vitro Inhibition of *Rb1* and *Meis2* in Adult Cardiomyocytes Induces Proliferation

First, we analyzed the differential expression of *Rb1* and *Meis2* between adult and neonatal hearts by Western blotting to evaluate the correlation of higher expression of *Rb1* and *Meis2* with the mature postmitotic state of cardiomyocytes. As expected from previous reports, both *Rb1* and *Meis2* were highly expressed in ACMs (12-week-old rats) compared with neonatal rat cardiomyocytes (24- to 48-hour-old rats) showing a 2.2- and a 2.9-fold increase, respectively (Figure 1A). Next, we optimized an isolation and culture protocol for ACMs from rats and validated a reproducible healthy culture efficacy assessed by quantifying live cardiomyocytes daily up to 7 days after the lipofectamine 2000 treatment (Figure 1B). Results showed that ACMs could be reliably cultured and maintained with over 59.57% of the total isolated ACMs remaining alive by day 7 after transfection (Figure S1). Similarly, to ensure a sufficient siRNA inhibition, we optimized our transfection protocol efficacy for ACMs using a scrambled control conjugated with the Dy547 fluorophore in a time course experiment. Utilizing the Dy547-conjugated *C. elegans*-miR-67 (*Cel*-miR-67), we were able to achieve over 70.16% transfection efficiency in ACMs at 24 hours after transfection (Figure S2) and observed over 70.0% transfection retention in ACMs by the siUBC-mediated transfection efficacy analysis at 48 hours (Figure S3). Following 7 days of specific siRNA knockdown against *Rb1* and *Meis2*, we observed protein levels reduced by 43% and 28%, respectively (Figure 1C through 1E). Individual and combinatory knockdowns of *Rb1* or *Meis2* revealed that the *Rb1* and *Meis2* combined knockdown approach, henceforth referred to as the "siRNA-cocktail" transfection, is necessary for the efficient induction of ACM proliferation with over 6-fold increase in EdU incorporation of ACMs in the siRNA-cocktail group compared with the individual *Rb1* and *Meis2* knockdown

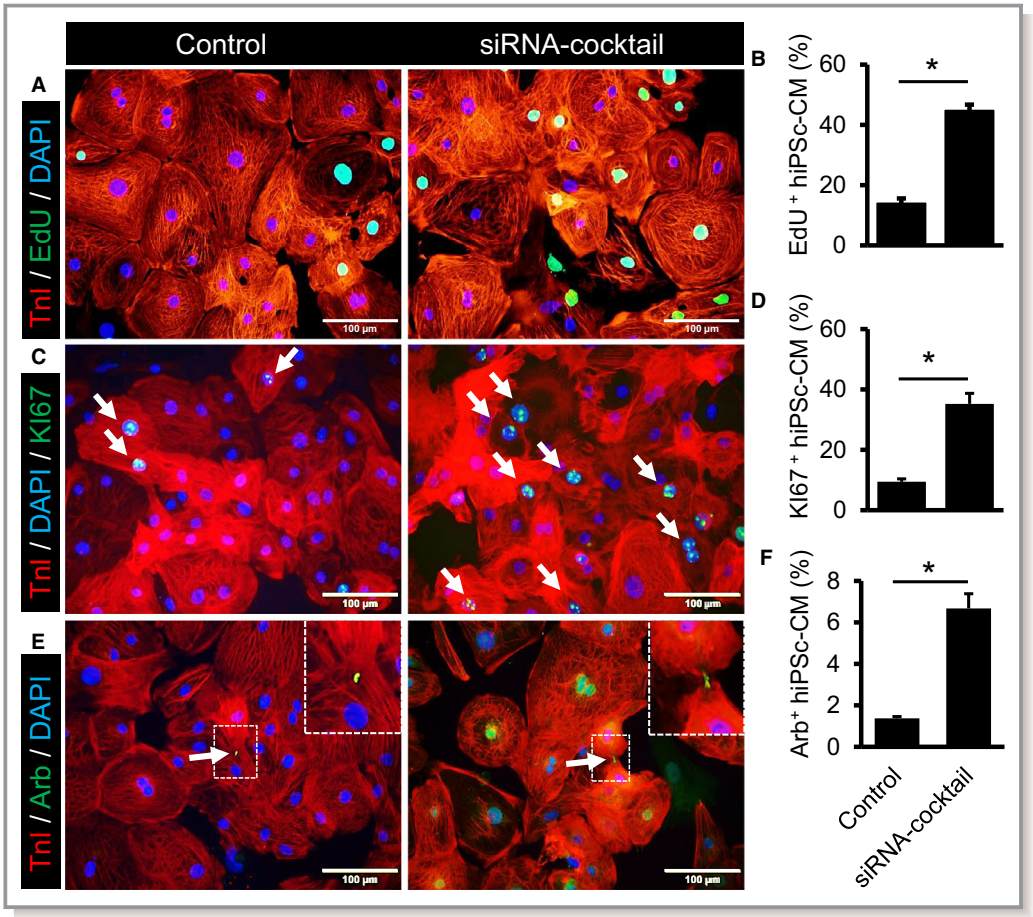

Figure 2. Simultaneous inhibition of *Rb1* and *Meis2* leads to hiPSc-CM proliferation. Representative immunostained images of hiPSc-CM showing a significant increase in (**A** and **B**) EdU-positive hiPSc-CM, (**C** and **D**) KI67-positive hiPSc-CM, and (**E** and **F**) Aurora B positive hiPSc-CM in the siRNA-cocktail–transfected group on day 5 after transfection vs control. Scale bar=100 µm. Panels in dashed rectangles represent respective enlarged sections. n=8 experimental replicates per group, and n=3 images each. Arb indicates Aurora B; DAPI, 4′,6-diamidino-2-phenylindole; EdU, 5-ethynyl-2′-deoxyuridine; hiPSc-CM, human induced pluripotent stem cell–derived cardiomyocytes; SEM, standard error of the mean; siRNA, short interfering RNA; TnI, Troponin I. Results are presented as mean±SEM; *$P \leq 0.05$. $P \leq 0.05$ was considered statistically significant.

experiments (Figure S4A). Further in vitro analysis of ACMs after simultaneous inhibition of *Rb1* and *Meis2* revealed a significant increase in cell numbers (32.8%) (Figure 1F and 1G) as well as a decrease in cell size (13.0%) (Figure 1H) when compared with controls. Additional analyses using all permutations of 3 independent sets of siRNAs against each *Rb1* and *Meis2* determined the optimum dose and set of siRNAs used in this study (Figure S4B). Moreover, time course analysis of nuclear composition of cultured cardiomyocytes between siRNA-cocktail–transfected group versus controls showed a significant increase in mononucleated ACMs (20.8% versus 14.4%) and a decrease in binucleated ACMs (75.1% versus 83.3%) (Figure S5A and S5B). Surprisingly, there was no significant difference in the number of multinucleated cells between the groups (Figure S5C). Because binucleated and multinucleated cardiomyocytes represent the terminally differentiated state,[41] the increase in mononucleated cardiomyocytes in the in vitro knockdown *Rb1* and *Meis2* experiments indicates newly formed cardiomyocytes.

Further time course analyses were performed based on the incorporation of EdU staining, indicating DNA synthesis, to evaluate the reentry of ACMs to the cell cycle. Results show that until day 5 after siRNA knockdown there is no detectable difference in the number of EdU-positive ACMs between experimental groups; however, on days 6 and 7, siRNA-cocktail–transfected groups have increased EdU labeling as opposed to control (32.7% versus 3.4% by day 7) (Figure 1I and 1J; Figure S6A and S6B). To ensure scoring proliferation specifically in ACM, triple antibody labeling was performed utilizing cardiomyocyte-specific markers, Nkx2.5 and TnI,

along with the EdU staining, and the cell cycle state in ACMs was determined. Immunostaining showed 26.05±1.28% of siRNA-cocktail–transfected ACMs with copositivity for cardiac markers and EdU, similar to the above data acquired by EdU counts alone (Figure S7).

To assess cell cycle progression to cytokinesis, siRNA-cocktail–transfected ACMs were labeled with a series of antibodies against cardiomyocyte marker TnI, DNA synthesis marker KI67, mitotic marker PH3, and cytokinesis marker Aurora B. Consistent with previous observations, transfected ACMs showed a significant increase in labeling for KI67 (19.8% versus 0.4%) (Figure 1K and 1L), PH3 (3.8% versus 0.2%) (Figure 1M and 1N), and Aurora B (3.3% versus 0%) (Figure 1O and 1P) in siRNA-cocktail–transfected groups compared with controls. Quantification of EdU, PH3, and TnI triple-labeled cardiomyocytes showed that all of the PH3-positive ACMs were also positive for EdU, and more than 82% of PH3-positive siRNA-transfected ACMs were, in fact, mononucleated, which is the evidence of completed cytokinesis (Figure S8).

Inhibition of *Rb1* and *Meis2* in ACMs Protects Against Cell Death

On evaluation of apoptotic cell death using the TUNEL assay, siRNA-cocktail–transfected ACMs showed a higher survival rate versus control group starting on day 3 and onward. In fact, by day 7, the siRNA-cocktail–transfected group maintains a significant decrease in TUNEL$^+$ ACMs (2.7±0.60%) compared with controls (6.13±0.68%) (Figure S9A and S9B). Additional cell death analysis is performed using Western blotting for a critical regulator of the apoptotic process, Bax, which was 0.56±0.10-fold lower in the proliferating ACMs (Figure S9C and S9D), validating the improved cell survival after siRNA-cocktail–mediated inhibition of *Rb1* and *Meis2*. Moreover, individual knockdown experiments in comparison to control or siRNA-cocktail transfection revealed that *Rb1* knockdown alone significantly protects ACM against cell death, as shown with the TUNEL assay (Figure S9E).

Rb1 and *Meis2* Combined Inhibition Enhances Proliferation in hiPSc-CMs

In a parallel experiment hiPSc-CMs were transfected with siRNA-cocktail or *Cel*-miR-67 control and analyzed for proliferation on day 5 after transfection. Human cardiomyocytes transfected with siRNAs showed a significant increase in EdU$^+$ labeling compared with controls (44.8% versus 14%) (Figure 2A and 2B). Moreover, a substantial number of hiPSc-CMs were positive for both *KI67* (35.2% versus 9.4%) (Figure 2C and 2D), and *Aurora B* (6.7% versus 1.4%) (Figure 2E and 2F) in siRNA-cocktail transfected groups.

Rb1 and *Meis2* Specific Inhibition Regulate Other Cell Cycle–Associated Genes In Vitro

RT-PCR and Western blot analyses in *Rb1/Meis2*-inhibited cells revealed that several cell cycle regulatory gene expressions were altered toward a proliferative state (Figure S10A). Genes inhibited by *Rb1* such as the *E2F* family members, transcription factors that are required for cell cycle progression, were upregulated, such as *E2F2* (4.1-fold) and *E2F3* (2.7-fold), in siRNA-cocktail–transfected ACMs (Figure S10A). Other critical cell cycle regulators such as *Cyclin D1* and *Aurora B* had significantly elevated expression levels (1.8- and 2.2-fold, respectively), whereas the expression of *IL6*, which is 1 of the most prominent cytokines to induce cell senescence by promoting DNA damage response, leading to cell cycle exit,[42] was reduced 0.2-fold in the siRNA-cocktail–transfected group (Figure S10A). Similarly, the expression level of a master regulator of proliferation such as *β-catenin* was up (1.9-fold) (Figure S10B and S10C), whereas the expression of a master regulator of senescence such as *P16* was down (0.7-fold) (Figure S10B and S10D) in the *Rb1/Meis2* knockdown group as shown by Western blot analyses.

Adult Cardiomyocytes Treated With siRNA-Cocktail In Vivo Following Ischemic Injury to the Heart Reenter Cell Cycle and Resist Cell Death in Peri-Infarct Areas

For all in vivo experiments, we used a model of myocardial infarction in adult (12-week-old) male Fischer 344 rats, performed by LAD ligation. siRNAs with nanocomposite hydrogel were injected at multiple sites in and around the infarcted area. We performed transthoracic echocardiography to assess heart function on days 3 and 21 before animals were euthanized on day 21, and heart samples were collected for further analysis (Figure 3A).

At first glance, physiological compensatory responses to injuries such as fibrosis in the infarcted area and the hypertrophy in the peri-infarct region of injured hearts were similar (Figure 3B). However, careful analyses and quantification of ACM size in the border zone of hearts treated with hydrogel+siRNA-cocktail showed a small but significant reduction of the hypertrophic response, in which ACMs remained smaller in size compared with no-treatment or hydrogel-alone controls (Figure 3B and 3C). Because intramyocardial injection treatment was administered at the site of LAD ligation, we assessed the ACM proliferation in peri-infarct areas of the adult rat heart through immunohistochemical staining. Similar to the in vitro studies, cell cycle marker *KI67* and cytokinesis-specific marker *Aurora B* showed a significantly higher number of *KI67*-positive (0.85% versus no treatment 0.15 and hydrogel 0.13) (Figure 3D and 3E) and

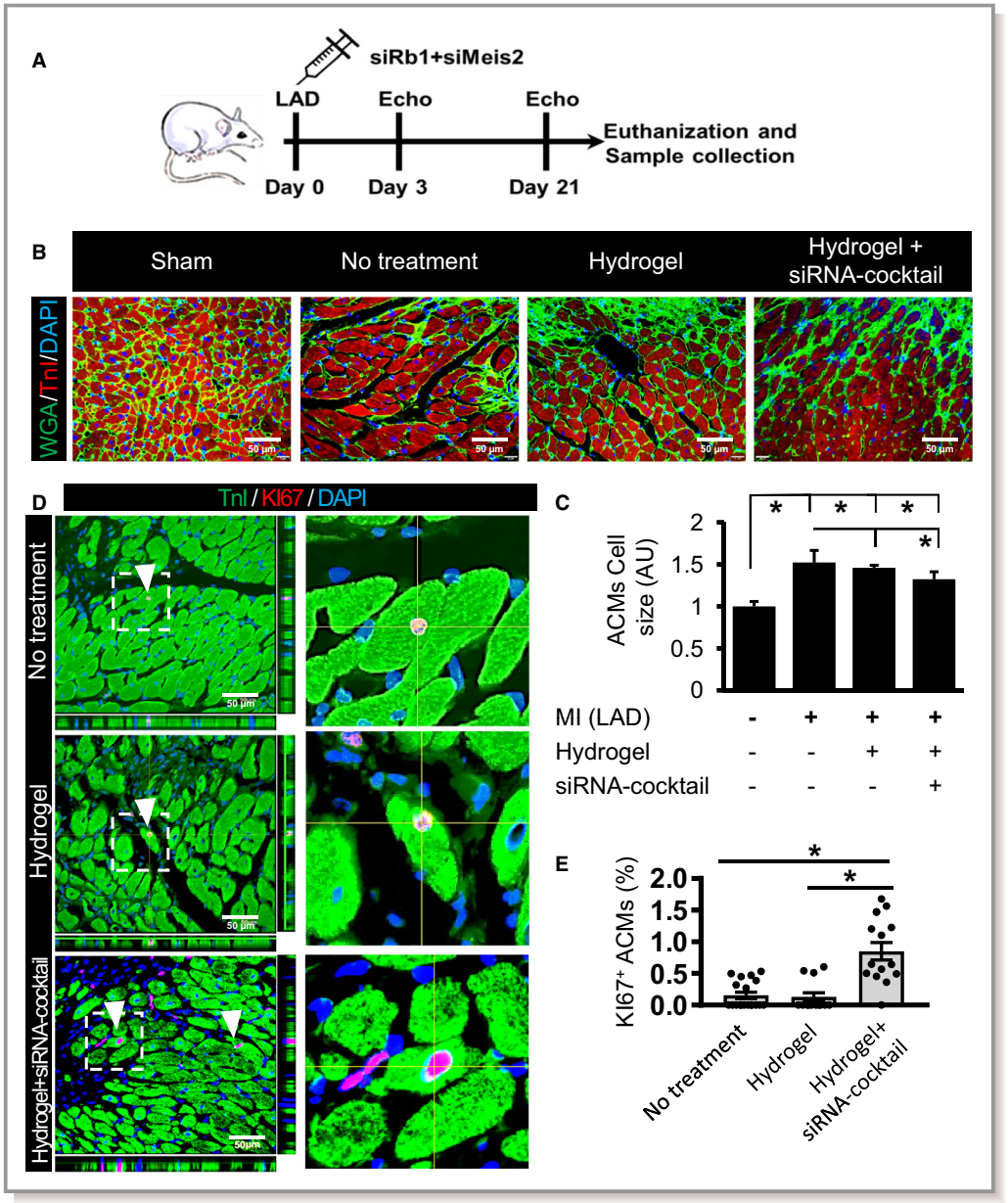

Figure 3. Hydrogel-mediated delivery of siRNA-cocktail leads to ACM proliferation in adult hearts post-MI. **A**, Schematic representation of in vivo experimental design, illustrating LAD ligation, intramyocardial injection of hydrogel, and hydrogel+siRNA-cocktail. Animals were observed for 21 days; echocardiography was performed at day 3 and day 21, followed by euthanasia and sample collection for molecular and histochemical analysis. **B**, Representative images for WGA staining (green) and troponin I (red) immunostaining. **C**, Quantification showing a moderate but significant decrease in ACM size in the siRNA-cocktail–transfected group when compared with controls. N=4 rats per group, n=5 nonserial sections were imaged from each, and n>100 cardiomyocytes quantified from each confocal image. **D**, Representative immunostaining images for TnI (green), KI67 (red), and DAPI (blue). **E**, Bar graphs show a significant increase in KI67-positive ACMs in the siRNA-cocktail–transfected group vs control. **F** and **G**, Representative images and bar graphs for immunostaining with Aurora B, showing a significant increase in Aurora B–positive ACMs in the siRNA-cocktail–transfected group vs control. In vivo analysis was performed in adult male rats (≈12 weeks old). N=4 rats per group, n=5 nonserial sections were imaged each, and n=8 confocal images from different regions quantified each. Scale bar=50 μm. ACM indicates adult cardiomyocyte; DAPI, 4′,6-diamidino-2-phenylindole; LAD, left anterior descending coronary artery; MI, myocardial infarction; si, short interfering [RNA]; TnI, Troponin I; WGA, wheat germ agglutinin. Results are presented as mean±SEM; *$P \leq 0.05$. $P \leq 0.05$ was considered as statistically significant.

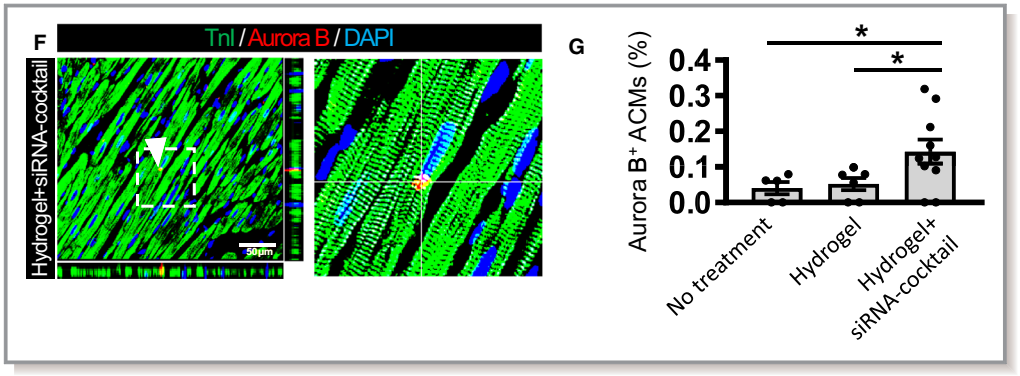

Figure 3. Continued.

Aurora B-positive (0.32% versus no treatment 0.04; and hydrogel 0.05) (Figure 3F and 3G) ACMs in the animals treated with hydrogel+siRNA-cocktail when compared with controls.

We also observed a significant decrease in the TUNEL$^+$ ACMs in the peri-infarcted area in the hydrogel+siRNA-cocktail–treated group (0.47±0.03%) versus controls (0.47% hydrogel+siRNA-cocktail versus 1.08% no treatment versus 0.98% hydrogel) (Figure S11A and 11B). These results demonstrate the improved survivability of ACMs in adult rat hearts treated with hydrogel+siRNA-cocktail when compared with controls.

We further validated our results by RT-PCR and Western blotting on heart tissue samples. The RT-PCR analysis confirmed the siRNA-mediated silencing of *Rb1* and *Meis2*, shown by a decreased expression of *Rb1* and *Meis2* and an increased expression of *E2F2* and *E2F3* in hydrogel+siRNA-cocktail–treated hearts (Figure S12). Moreover, our RT-PCR analysis revealed an elevated level of *Aurora B* and a decreased level of *IL6*, whereas we could not find any difference in *Cyclin D1* expression in vivo (Figure S12). Comparable results were obtained in our Western blot analysis, in which we observed a reduced expression of *Meis2* and *p16* in the hydrogel+siRNA-cocktail–treated group in comparison to control groups, which further complements our RT-PCR results (Figure S13A through S13C). The results collectively ascertain that siRNA-mediated inhibition of *Rb1* and *Meis2* leads to ACM proliferation in adult rat hearts post-MI.

Rb1 and *Meis2* Knockdown in ACM Results in Requisition of Cell-Autonomous Proangiogenic Properties After MI or In Vitro

Previous studies have suggested a potential role for *Rb1* in angiogenesis during development and disease.[43,44] In the present study we evaluated the proangiogenic effects of inhibiting *Rb1* and *Meis2* in adult animals following MI. Histological analyses showed an increase in blood vessel density in the hydrogel+siRNA-cocktail–treated group (21.8% hydrogel+siRNA-cocktail versus 12.0% no treatment versus 15.0% hydrogel only) (Figure 4A and 4B). To determine whether ACMs directly regulate this enhanced angiogenesis after the inhibition of *Rb1/Meis2*, we performed endothelial tube formation assays in vitro. Here, we cultured HUVECs with conditioned medium from ACMs transfected with siRNA-cocktail (CMe-siRNA-cocktail) and medium from ACMs transfected with *Cel*-miR-67 (CMe-control) (Figure 4C). Interestingly, we observed a significant increase in the total number of tubes (136±12.1 versus 84±4.9) as well as the length (20 973±404 μm versus 17 575±58 μm) and number of branching points per tube formation (65.75±1.93 versus 51±1.6) in the HUVECs cultured with CMe-siRNA-cocktail in comparison to CMe-control (Figure 4D through 4G). RT-PCR and Western blot analyses of a critical angiogenic vascular endothelial growth factor showed a significant increase in expression in the hydrogel+siRNA-cocktail–treated group compared with controls post-MI (Figure S12).

In contrast, cardiac fibroblasts and endothelial cells transfected with either individual siRNAs or siRNA-cocktail did not show any enhancements in proliferation or survival and did not alter HUVEC cultures (Figure S14A through S14C). Meanwhile, neonatal rat cardiomyocytes, which pose a baseline proliferative capacity, acquired a significantly improved proliferative state on siRNA-cocktail transfection (Figure S14D).

Inhibition of *Rb1* and *Meis2* Following MI Is Cardioprotective

Echocardiographic measurement analyses of uninjured, healthy adult rats that received an intramyocardial injection of either 100 μL of hydrogel alone or PBS showed no baseline functional improvement up to 3 weeks postinjection (Figure S15). Similarly, infarcted hearts that were injected with *Rb1/Meis2* siRNA-infused hydrogel following MI did not alter

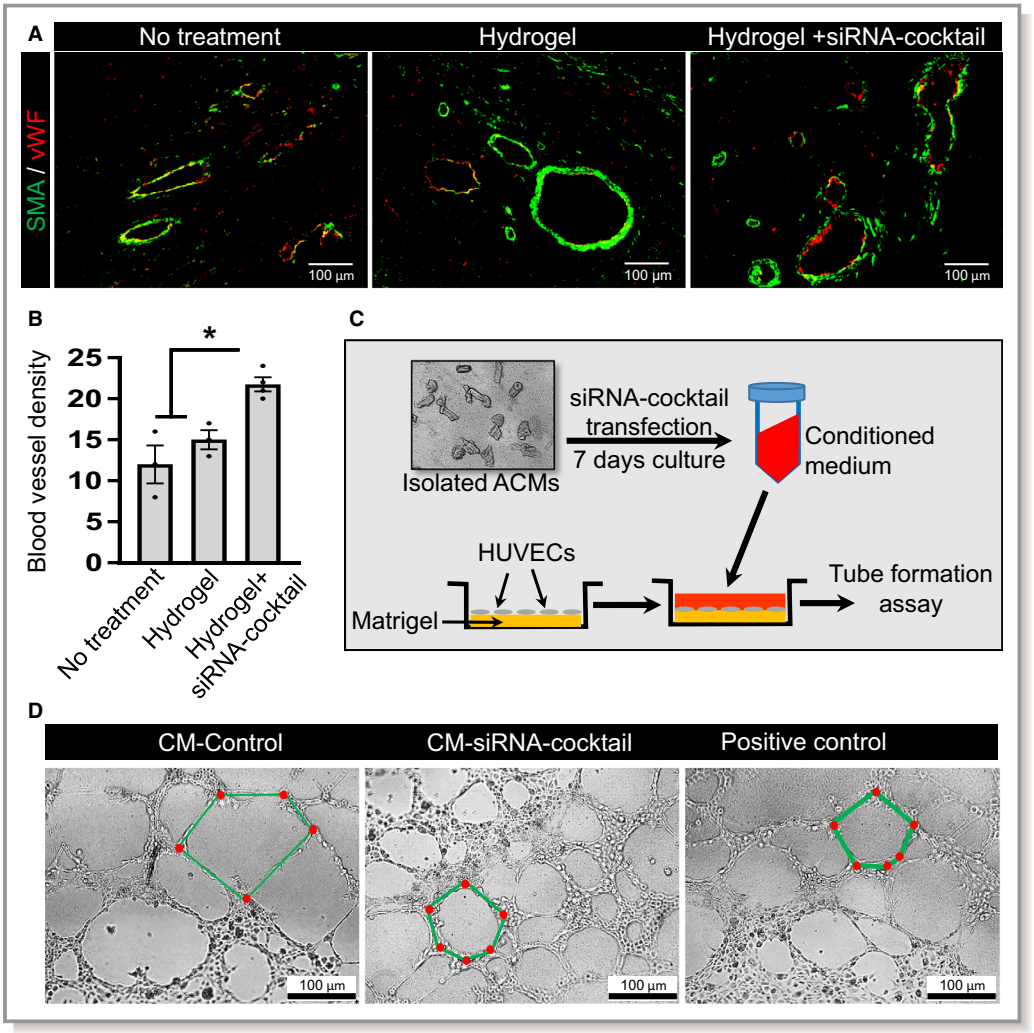

Figure 4. Hydrogel-mediated delivery of siRNA-cocktail leads to increased vascularization in adult animals post-MI. **A**, Representative immunostaining images for blood vessel density in different study groups: the inner endothelial layer is visualized by von Willebrand factor (vWF) staining (red), whereas the outer layer is visualized by smooth muscle actin (SMA) staining (green). **B**, Quantification of blood vessel density shows a significant increase in the siRNA-cocktail–treated group when compared with controls. N=4 rats per group, n=5 nonserial sections were imaged from each, and n=3 confocal images from different regions quantified each. **C**, Schematic representation of tube formation assay, illustrating ACM transfection and conditioned medium (CM) isolation, which was used to culture HUVECs and the subsequent tube formation assay. **D**, Representative bright-field images for endothelial tube formation assay in HUVECs illustrate the increase in total number of tubes, total tube length, and number of branching points in the siRNA-cocktail group vs control. **E-G**, Quantification of endothelial tube formation was performed by Wimasis image analysis tool (2017; WimTube: Tube Formation Assay Image Analysis Solution, Release 4.0; Onimagin Technologies, Córdoba, Spain). Significant increases in total number of tubes, total tube length, and number of branching points were observed. Images represent N=3 rats, n=6 experimental replicates each, and n=5 images quantified each. Scale bar=100 µm. ACM indicates adult cardiomyocytes; HUVEC, human umbilical vein endothelial cells; siRNA, short interfering RNA; SMA, α-smooth muscle actin; vWF, von Willebrand factor. Results are presented as mean±SEM; *$P \leq 0.05$. $P \leq 0.05$ was considered statistically significant.

the heart weight/body weight ratio compared with both hydrogel alone and PBS control groups (Figure 5A). However, hearts receiving the *Rb1/Meis2* siRNA-infused hydrogel exhibited a substantially reduced infarct size measured by Masson trichrome staining at 21 days postinjury (Figure 5B and 5C). As expected, these siRNA-treated hearts displayed improved cardiac function as seen from ejection fraction, cardiac output, and LV systolic internal dimension values at

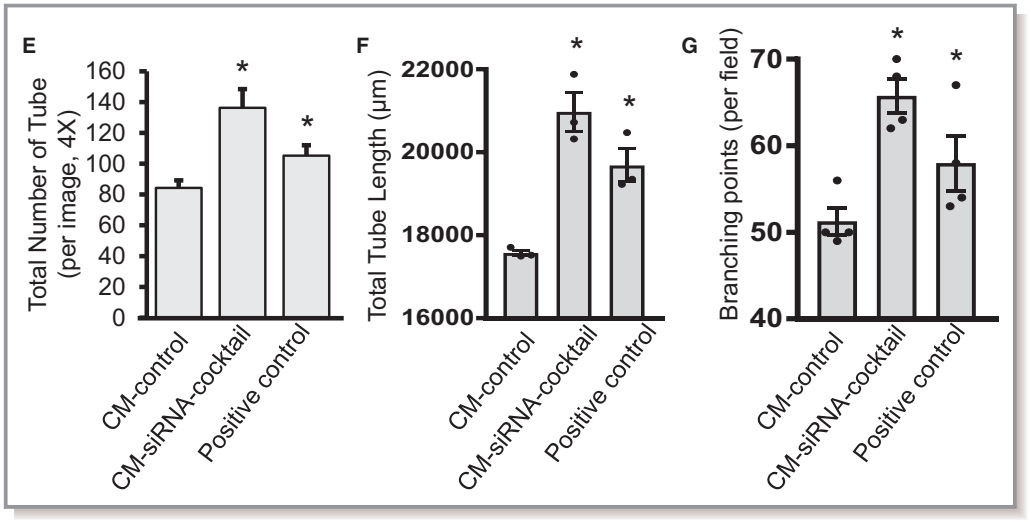

Figure 4. Continued.

day 21 compared with either control group (Figure 5D through 5I). We also observed a significant improvement in radial strain, radial strain rate, radial displacement, and radial velocity within the siRNA-infused hydrogel-treated group (Figure 5J through 5L, Figure S16). Interestingly, during the early stages of injury recovery at day 3 after injury, hearts that received hydrogel alone showed significant functional protection seen from early echocardiography measurements (Figure 5G through 5I); this was also apparent from the scar size but lacked significance at day 21 post-MI (Figure 5B and 5C). These results demonstrate that hydrogel-mediated delivery of siRNA-cocktail following MI prevents cardiac remodeling and improves heart function.

Discussion

In the present study,we highlight a promising cardioprotective treatment approach by utilizing the siRNA-infused hydrogel injection directly to the injury site after an ischemic heart injury. More specifically, we inhibited a set of actively expressed cell senescence inducers, *Rb1*, and *Meis2*, which in return effectively induced terminally differentiated, postmitotic, ACMs to reenter the cell cycle. Remarkably, these reactivated cycling ACMs acquired antiapoptotic and proangiogenic properties, provided significant cardioprotection, and led to improved wound healing and cardiac function following myocardial infarct. This study builds on top of our group's previous findings wherein we reported induced cardiomyocyte proliferation on overexpressing miR-1825, which we suggested to regulate a known proliferation-inducing miRNA, miR-199a, with a potential mechanism of silencing *Rb1* or *Meis2* expression.[37] We also showed that *Rb1* and *Meis2* are direct targets of miR-199a with a specific binding site on 3′UTR.[37] In our previous study we also explored the potential of direct silencing of *Rb1* and *Meis2* in vitro and showed signs of cardiomyocyte proliferation with a synergetic relation between *Rb1* and *Meis2*.[37] The present study, now for the first time, shows the efficacy of induced ACM proliferation through the simultaneous repression of *Rb1* and *Meis2* using a siRNA approach both in vitro transfection experiments and in vivo by using a hydrogel-based delivery method that remarkably improved cardiac function after MI.

Because *Rb1* and *Meis2* are associated with different stages of the cell cycle,[20,22,32,45,46] and on the basis of our previous observations, we proposed a simultaneous inhibition protocol for *Rb1* and *Meis2* to induce ACM proliferation and to avoid mitotic catastrophe.[42] Mitotic catastrophe is a phenomenon in which karyokinesis occurs with incomplete cytokinesis leading to ACM apoptosis.[47] As reported before, isolated and cultured adult rat cardiac myocytes exhibit changes in their external and internal structural properties differentiating from their typical in vivo rod shape to a more pleiomorphic, flattened, and adherent neonatal-like phenotype.[48] Our in vitro studies using developmentally mature ACMs isolated from adult male rats also showed a remarkable morphological change but retained their physiological and contractile characteristics in culture even up until day 7 (Video S1). During that time window we were able to achieve a transfection efficiency of >70% in the ACMs, resulting in over 50% reduction in mRNA expression of both targeted genes. Consequently, we observed a remarkable increase in mononucleated ACM numbers with a decrease in cell size in the siRNA-cocktail–transfected group. Surprisingly the induced ACM proliferation was only possible with simultaneous inhibition of *Rb1* and *Meis2,* whereas separate inhibition of these genes did not result in much proliferation. This was interesting because simple knockout of a previously identified transcription factor,

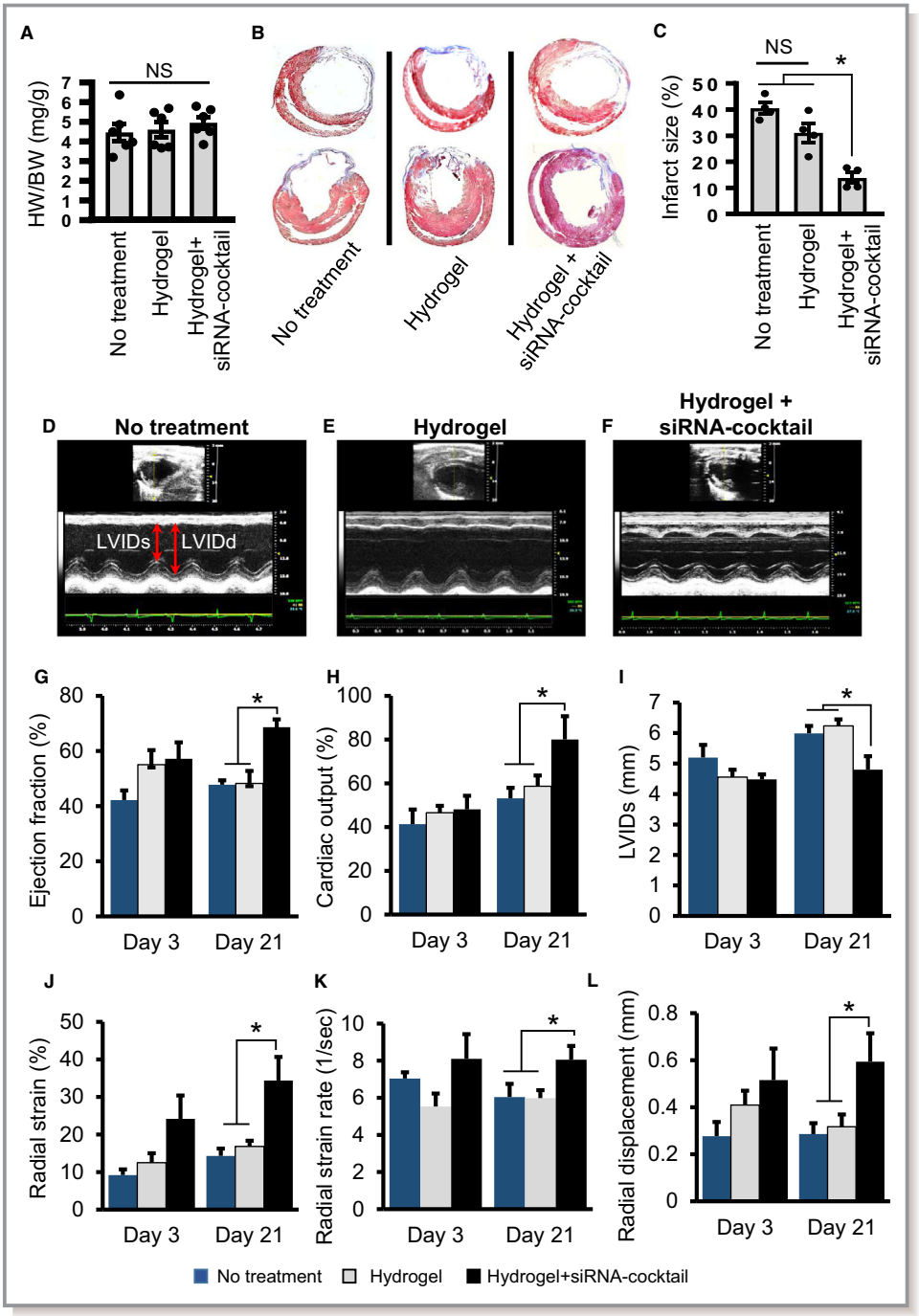

Figure 5. Hydrogel-mediated delivery of siRNA-cocktail leads to a reduction in infarct size and improved cardiac function post-MI. **A**, No significant difference was observed in heart weight–to–body weight ratio between the groups. **B** and **C**, Representative images for Masson trichrome staining show a significant reduction in infarct size after siRNA-cocktail treatment in adult animals post-MI. N=6 rats per group; n=5 nonserial sections were imaged each. **D** through **F**, Representative echocardiography images of heart function analysis at the long axis and M-mode. **G** through **L**, Quantification of echocardiography shows significantly improved EF, CO, LVIDs, radial strain, radial strain rate, and radial displacement in the siRNA-cocktail–treated group in comparison to controls. In vivo analysis of cardiac function was performed in adult male rats (≈12 weeks old). Results represent N=6 rats per group. BW indicates body weight; CO, cardiac output; EF, ejection fraction; HW, heart weight; LVIDd, left ventricular internal dimension, diastole (mm); LVIDs, left ventricular internal dimension, systole (mm); NS, nonsignificant; siRNA, short interfering RNA. Results are presented as mean±SEM; *$P \leq 0.05$. NS=$P \geq 0.05$. $P \leq 0.05$ was considered as statistically significant.

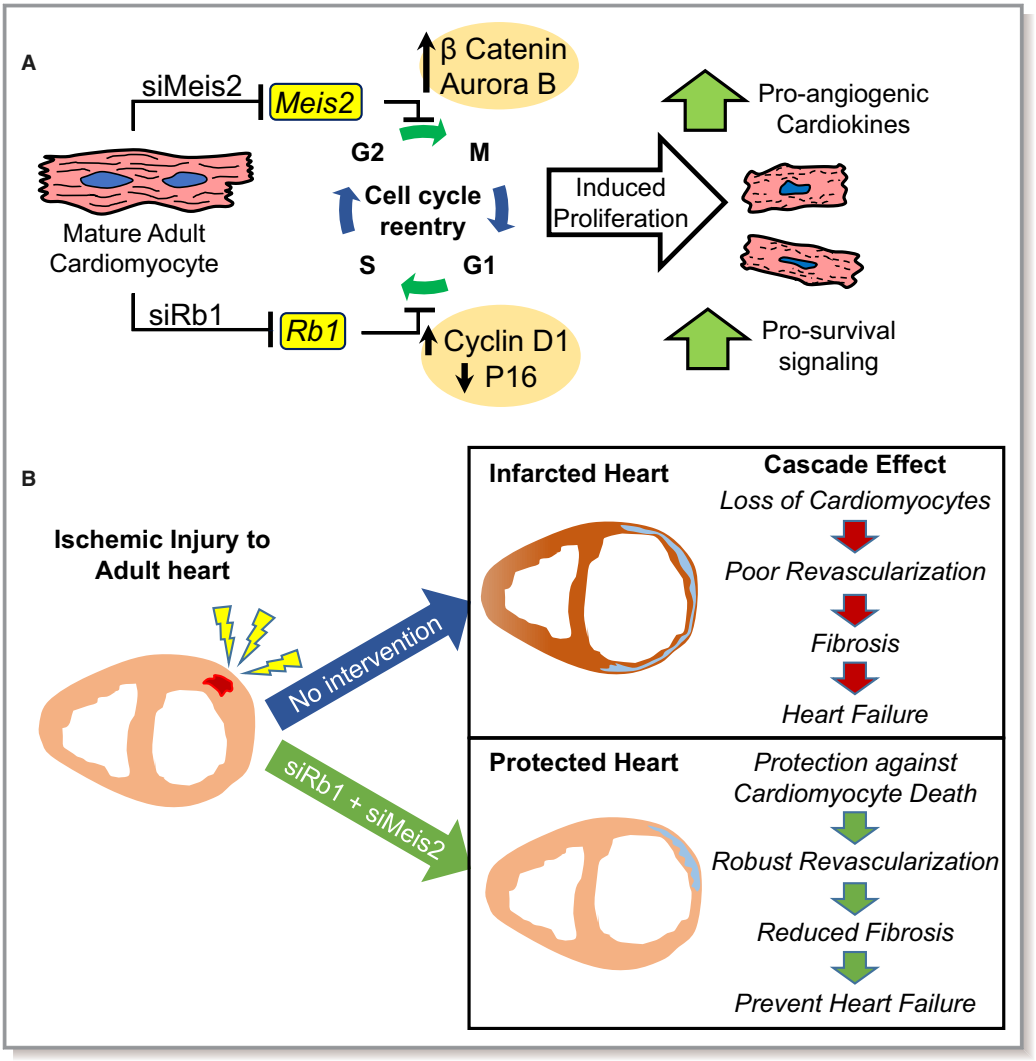

Figure 6. Simultaneous inhibition of *Rb1* and *Meis2* leads to ACM cell cycle progression and cardioprotection post-MI. **A,** Schematic representation of siRNA-mediated simultaneous inhibition of *Rb1* and *Meis2*, showing induced entry to S phase by siRb1-mediated silencing *Rb1*. *Mies2* inhibition facilitates mitosis, which collectively leads to induced ACM proliferation. The differential expression of Aurora B, β-catenin, cyclin D1, and p16 are complementary to the induced ACM proliferation after *Rb1* and *Meis2* inhibition. **B**, The cascade of events that occur when an ischemic injury to the heart that leads to heart failure is significantly reversed or prevented by an *Rb1* and *Meis2* knockdown approach. More significant than ACM proliferation, protection against cardiomyocyte death and cardiomyocyte-mediated enhanced angiogenesis protect the heart from progressive myocardial loss, reduce fibrosis, and restore function in an adult animal post-MI. ACM indicates adult cardiomyocytes; MI, myocardial infarction; si-, short interfering [RNA].

Meis1, which had been determined to be the master activator of the cyclin-dependent kinase inhibitors, results in a dramatic enhancement of ACM proliferation.[49] The difference in the mechanism by which *Meis1* and *Rb1/Meis2* induces ACM proliferation revealed an alternative cardioprotective phenomenon in our study.

Rb1 negatively regulates the cell cycle by interacting with transcription factors *E2F2* and *E2F3* and thus inhibiting the synthesis phase.[26,27] After siRNA-cocktail–mediated inhibition of *Rb1, we* observed a significant increase in the expression of *E2F2* and *E2F3* along with an increase in DNA synthesis marked by a 10-fold increase in EdU incorporation. Our results here specifically focus on the cardiomyocyte proliferation with a triple colabeling of cardiomyocyte-specific markers Nkx2.5 and TnI along with the EdU, Ph3, KI67, and Aurora B to present compelling evidence for cardiomyocyte reentry to the cell cycle. Compiling accounts of upregulation in cell cycle promoters such as *cyclin D1* and *β-catenin* and downregulation of cell cycle inhibitors *p16* and *IL6*, as a result of siRNA-mediated inhibition of *Rb1* and *Meis2*, the almost

perfect colocalization of the synthesis marker EdU with mitotic marker PH3 in mononucleated ACM (Figure S8), and live cell imaging (Figure S17) all verified adult cardiomyocyte cytokinesis. As an additional benefit, siRNA-cocktail–transfected ACMs showed a 2-fold decrease in apoptosis, which may give the ACMs a boost in their ability to enter the cell cycle with increased survivability. Together, our in vitro results indicate that siRNA mediated simultaneous inhibition of *Rb1*- and *Meis2*-induced ACM proliferation and increased ACM survivability.

In addition to our data within murine cardiomyocytes, we also showed substantial induction of proliferation in hiPSc-CM with the same siRNA-cocktail transfection, documenting a conserved mechanism between species and highlighting the clinical relevance of siRNA-cocktail–induced inhibition of *Rb1* and *Meis2* as therapeutics.

In this study we evaluated the therapeutic significance of exogenous induction of ACM proliferation in a murine model of acute ischemic myocardial infarction through a permanent ligation surgery on the left anterior descending artery (LAD) in adult rats.[50,51] Immediately after LAD ligation, siRNA cocktail was injected into the peri-infarct area surrounding the injury site. Currently, localized drug delivery in heart disease is a challenging task, and common delivery routes have limitations such as off-target effects and low retention. To overcome these limitations, we used a chemically modified nanocomposite hydrogel as the delivery vehicle for intramyocardial injection of the siRNA cocktail. Nanocomposite hydrogels have been emerging as an advanced tool in tissue engineering and regenerative medicine for their ability to carry drugs and growth factors.[52-55] Moreover, hydrogel injection has the advantage of site-specific delivery of even minimal amounts of drugs with a sustained-release property, making them more efficient and feasible compared with tail vein injections.[56-58] Our chemically modified biocompatible silicate-based hydrogel was designed and characterized for biocompatibility and sustained-release kinetics, which was described earlier.[38,39] The present study further analyzes the in vivo application of this hydrogel and its delivery properties to evaluate its employment toward intramyocardial injection treatment both in uninjured and injured myocardium. Our biocompatible hydrogel, when injected into healthy adult rats, showed no consequence to the function or morphology of the hearts, which was promising for the accurate assessment of the potential effects of siRNAs. Interestingly, however, if hydrogel alone, without any siRNAs, is injected into the infarct region after injury, we observed a robust but transient cardioprotection most apparent during the early acute phase of myocardial remodeling. In agreement with our observation, several other studies recently report beneficial effects of intramyocardial injection of biomaterials that are thought to provide mechanical support to the myocardium after injury or after a massive loss of cardiomyocytes.[59-61] However, the manner by which hydrogels act as a cardioprotection will be determined with careful cell-specific interrogations on hydrogel injection; it remains to be determined in our and other future studies.

Even so, hydrogel-mediated delivery of siRNA-cocktail knocking down *Rb1* and *Meis2* revealed a much more significant reduction in infarct size compared with hydrogel alone that lasted past 3 weeks post-MI with an all-around recovery of cardiac function. Advanced echocardiographic measurement analyses with global and regional strain and strain rate imaging showed a considerable improvement in LV systolic internal dimension, ejection fraction, radial strain, radial strain rate, radial displacement, and radial velocity, and thus, improved cardiac output in siRNA-cocktail–treated adult rat post-MI. As expected from our in vitro data, immunohistochemical analysis revealed a significant increase in ACMs in the cell cycle, as detected by a larger number of ACMs positive for KI67 and Aurora B in siRNA-cocktail–treated animal hearts post-MI. RT-PCR and Western blot analyses for proliferation markers support the induced proliferation of ACMs in hearts after MI in the *Rb1/Meis2* siRNA-cocktail–treated group. Modest changes detected in the expression levels for cell cycle–associated genes in RT-PCR and Western blot analyses compared with the substantial increase in cell proliferation scored in histological assessment result from the difference in sample preparation and scoring methods. RT-PCR and Western blot analyses were performed on whole-heart tissue digests; meanwhile, immunofluorescent analysis was performed within the peri-infarct region. This observation is indicative of a successful injury site–specific silencing of *Rb1* and *Meis2,* which spares the uninjured areas of the heart from unintended, possibly pathological hyperplasia, potentially permitting repeated treatments with the lack of off-target and off-site effects.

The principal aim of this study was to induce cardiomyocyte proliferation in order to replenish lost myocytes after myocardial infarct, and we did observe a significant induction of ACM proliferation in vitro and in vivo. However, the number of new cardiomyocytes we accumulated either in cell culture or in vivo cannot feasibly replace the massive loss of myocardium after an ischemic event or explain the preservation of cardiac output.

In fact, we believe that the robust phenotype we observe in vivo is mostly due to a secondary cardioprotective phenomenon resulting from ACMs reentering the cell cycle and acquiring antiapoptotic and proangiogenic properties. Inhibition of *Rb1* and *Meis2* protected cardiomyocytes against ischemic injury with a remarkable 50% reduction in cell death compared with controls. Moreover, reactivated and potentially rejuvenated cardiomyocytes acquired a proangiogenic secretome facilitating a significant increase in the vessel density

after myocardial injury, which coincides with previous reports that angiogenesis is transcriptionally regulated through the *Rb1-E2F* axis.[43,44]

Our present study establishes that a terminally differentiated cardiomyocyte can reenter the cell cycle with a siRNA-mediated inhibition of *Rb1* and *Meis2* in vitro and in vivo and consequently improve cardiac repair, function, and angiogenesis in adult mammalian hearts following an acute ischemic injury (Figure 6). Altogether, this study highlights a novel therapeutic potential for stimulated cardiomyocyte cell-cycle reentry and proliferation employing a site-targeted injection treatment of cardiac injuries via siRNA-infused hydrogels. However, extensive analyses using genetic mouse models of lineage tracing, gain and loss of function studies utilizing fluorescence-activated cell sorting, single-cell RNA sequencing, single-cell proteomics, and secretome analyses will determine the therapeutic potential of ACM reactivation and rejuvenation and will lead to novel therapeutics.

Acknowledgments

The senior author thanks all the people who have supported the design and execution of this study. The authors would like to thank Birgit Ehmer, PhD, and the Center for Biological Microscopy located in Department of Cancer Biology, Vontz Center for Molecular Studies, University of Cincinnati, for their help and expertise in acquiring live cell images.

Sources of Funding

This work was supported by funding from the Department of Pathology and Laboratory Medicine, University of Cincinnati, College of Medicine, to Dr Onur Kanisicak; a grant from the National Institutes of Health (HL106190-01) to Dr Rafeeq Habeebahmed, and a grant from the National Institute of General Medical Sciences (P20GM103638) to Dr Arghya Paul. Dr Sakthivel Sadayappan has received support from the National Institutes of Health (R01HL130356, R01HL105826, and R01/R56HL139680) as well as from AstraZeneca, Merck, and Amgen. Dr Onur Kanisicak is supported by the American Heart Association Career Development Award (18CDA34110117).

Disclosures

Dr Sadayappan has provided consulting and collaborative services to AstraZeneca, Merck, and Amgen unrelated to the content of this article. The remaining authors have no disclosures to report.

References

1. Tousoulis D, Androulakis E, Kontogeorgou A, Papageorgiou N, Charakida M, Siama K, Latsios G, Siasos G, Kampoli AM, Tourikis P, Tsioufis K, Stefanadis C. Insight to the pathophysiology of stable angina pectoris. *Curr Pharm Des*. 2013;19:1593–1600.
2. Vagnozzi RJ, Molkentin JD, Houser SR. New myocyte formation in the adult heart: endogenous sources and therapeutic implications. *Circ Res*. 2018;123:159–176.
3. Maliken BD, Kanisicak O, Karch J, Khalil H, Fu X, Boyer JG, Prasad V, Zheng Y, Molkentin JD. Gata4-dependent differentiation of c-Kit(+)-derived endothelial cells underlies artefactual cardiomyocyte regeneration in the heart. *Circulation*. 2018;138:1012–1024.
4. Li Y, He L, Huang X, Bhaloo SI, Zhao H, Zhang S, Pu W, Tian X, Li Y, Liu Q, Yu W, Zhang L, Liu X, Liu K, Tang J, Zhang H, Cai D, Ralf AH, Xu Q, Lui KO, Zhou B. Genetic lineage tracing of nonmyocyte population by dual recombinases. *Circulation*. 2018;138:793–805.
5. van Amerongen MJ, Engel FB. Features of cardiomyocyte proliferation and its potential for cardiac regeneration. *J Cell Mol Med*. 2008;12:2233–2244.
6. Wang J, Panakova D, Kikuchi K, Holdway JE, Gemberling M, Burris JS, Singh SP, Dickson AL, Lin YF, Sabeh MK, Werdich AA, Yelon D, Macrae CA, Poss KD. The regenerative capacity of zebrafish reverses cardiac failure caused by genetic cardiomyocyte depletion. *Development*. 2011;138:3421–3430.
7. Parente V, Balasso S, Pompilio G, Verduci L, Colombo GI, Milano G, Guerrini U, Squadroni L, Cotelli F, Pozzoli O, Capogrossi MC. Hypoxia/reoxygenation cardiac injury and regeneration in zebrafish adult heart. *PLoS One*. 2013;8:e53748.
8. Gonzalez-Rosa JM, Martin V, Peralta M, Torres M, Mercader N. Extensive scar formation and regression during heart regeneration after cryoinjury in zebrafish. *Development*. 2011;138:1663–1674.
9. Omatsu-Kanbe M, Nozuchi N, Nishino Y, Mukaisho KI, Sugihara H, Matsuura H. Identification of cardiac progenitors that survive in the ischemic human heart after ventricular myocyte death. *Sci Rep*. 2017;7:41318.
10. Tian J, An X, Niu L. Role of microRNAs in cardiac development and disease. *Exp Ther Med*. 2017;13:3–8.
11. Pandey R, Yang Y, Jackson L, Ahmed RP. MicroRNAs regulating meis1 expression and inducing cardiomyocyte proliferation. *Cardiovasc Regen Med*. 2016;3:e1468.
12. Kimura W, Xiao F, Canseco DC, Muralidhar S, Thet S, Zhang HM, Abderrahman Y, Chen R, Garcia JA, Shelton JM, Richardson JA, Ashour AM, Asaithamby A, Liang H, Xing C, Lu Z, Zhang CC, Sadek HA. Hypoxia fate mapping identifies cycling cardiomyocytes in the adult heart. *Nature*. 2015;523:226–230.
13. Pawlikowski JS, Adams PD, Nelson DM. Senescence at a glance. *J Cell Sci*. 2013;126:4061–4067.
14. Rayess H, Wang MB, Srivatsan ES. Cellular senescence and tumor suppressor gene p16. *Int J Cancer*. 2012;130:1715–1725.
15. Maejima Y, Adachi S, Ito H, Hirao K, Isobe M. Induction of premature senescence in cardiomyocytes by doxorubicin as a novel mechanism of myocardial damage. *Aging Cell*. 2008;7:125–136.
16. Serrano M, Lin AW, McCurrach ME, Beach D, Lowe SW. Oncogenic ras provokes premature cell senescence associated with accumulation of p53 and p16INK4a. *Cell*. 1997;88:593–602.
17. Mohamed TMA, Ang YS, Radzinsky E, Zhou P, Huang Y, Elfenbein A, Foley A, Magnitsky S, Srivastava D. Regulation of cell cycle to stimulate adult cardiomyocyte proliferation and cardiac regeneration. *Cell*. 2018;173:104–116.e12.
18. Bergmann O, Bhardwaj RD, Bernard S, Zdunek S, Barnabe-Heider F, Walsh S, Zupicich J, Alkass K, Buchholz BA, Druid H, Jovinge S, Frisen J. Evidence for cardiomyocyte renewal in humans. *Science*. 2009;324:98–102.
19. Wang LL, Liu Y, Chung JJ, Wang T, Gaffey AC, Lu M, Cavanaugh CA, Zhou S, Kanade R, Atluri P, Morrisey EE, Burdick JA. Local and sustained miRNA delivery from an injectable hydrogel promotes cardiomyocyte proliferation and functional regeneration after ischemic injury. *Nat Biomed Eng*. 2017;1:983–992.
20. Hille S, Dierck F, Kuhl C, Sosna J, Adam-Klages S, Adam D, Lullmann-Rauch R, Frey N, Kuhn C. Dyrk1a regulates the cardiomyocyte cell cycle via D-cyclin-dependent Rb/E2f-signalling. *Cardiovasc Res*. 2016;110:381–394.
21. Takebayashi S, Tanaka H, Hino S, Nakatsu Y, Igata T, Sakamoto A, Narita M, Nakao M. Retinoblastoma protein promotes oxidative phosphorylation through upregulation of glycolytic genes in oncogene-induced senescent cells. *Aging Cell*. 2015;14:689–697.
22. Jiang Z, Zacksenhaus E, Gallie BL, Phillips RA. The retinoblastoma gene family is differentially expressed during embryogenesis. *Oncogene*. 1997;14:1789–1797.
23. MacLellan WR, Garcia A, Oh H, Frenkel P, Jordan MC, Roos KP, Schneider MD. Overlapping roles of pocket proteins in the myocardium are unmasked by germ line deletion of p130 plus heart-specific deletion of Rb. *Mol Cell Biol*. 2005;25:2486–2497.

24. Puente BN, Kimura W, Muralidhar SA, Moon J, Amatruda JF, Phelps KL, Grinsfelder D, Rothermel BA, Chen R, Garcia JA, Santos CX, Thet S, Mori E, Kinter MT, Rindler PM, Zacchigna S, Mukherjee S, Chen DJ, Mahmoud AI, Giacca M, Rabinovitch PS, Aroumougame A, Shah AM, Szweda LI, Sadek HA. The oxygen-rich postnatal environment induces cardiomyocyte cell-cycle arrest through DNA damage response. *Cell*. 2014;157:565–579.
25. Vara D, Bicknell KA, Coxon CH, Brooks G. Inhibition of E2F abrogates the development of cardiac myocyte hypertrophy. *J Biol Chem*. 2003;278:21388–21394.
26. Hiebert SW, Chellappan SP, Horowitz JM, Nevins JR. The interaction of RB with E2F coincides with an inhibition of the transcriptional activity of E2F. *Genes Dev*. 1992;6:177–185.
27. Cao L, Peng B, Yao L, Zhang X, Sun K, Yang X, Yu L. The ancient function of RB-E2F pathway: insights from its evolutionary history. *Biol Direct*. 2010;5:55.
28. Busk PK, Bartkova J, Strom CC, Wulf-Andersen L, Hinrichsen R, Christoffersen TE, Latella L, Bartek J, Haunso S, Sheikh SP. Involvement of cyclin D activity in left ventricle hypertrophy in vivo and in vitro. *Cardiovasc Res*. 2002;56:64–75.
29. Kirshenbaum LA, Abdellatif M, Chakraborty S, Schneider MD. Human E2F-1 reactivates cell cycle progression in ventricular myocytes and represses cardiac gene transcription. *Dev Biol*. 1996;179:402–411.
30. Lowe SW, Cepero E, Evan G. Intrinsic tumour suppression. *Nature*. 2004;432:307–315.
31. Bhanvadia RR, VanOpstall C, Brechka H, Barashi NS, Gillard M, McAuley EM, Vasquez JM, Paner G, Chan WC, Andrade J, De Marzo AM, Han M, Szmulewitz RZ, Vander Griend DJ. MEIS1 and MEIS2 expression and prostate cancer progression: a role for HOXB13 binding partners in metastatic disease. *Clin Cancer Res*. 2018;24:3668–3680.
32. Bjerke GA, Hyman-Walsh C, Wotton D. Cooperative transcriptional activation by Klf4, Meis2, and Pbx1. *Mol Cell Biol*. 2011;31:3723–3733.
33. Jiang S, Haider HK, Idris NM, Salim A, Ashraf M. Supportive interaction between cell survival signaling and angiocompetent factors enhances donor cell survival and promotes angiomyogenesis for cardiac repair. *Circ Res*. 2006;99:776–784.
34. Pandey R, Ahmed RP. MicroRNAs inducing proliferation of quiescent adult cardiomyocytes. *Cardiovasc Regen Med*. 2015;2:e519.
35. Arif M, Pandey R, Alam P, Jiang S, Sadayappan S, Paul A, Ahmed RPH. MicroRNA-210-mediated proliferation, survival, and angiogenesis promote cardiac repair post myocardial infarction in rodents. *J Mol Med (Berl)*. 2017;95:1369–1385.
36. Lesizza P, Prosdocimo G, Martinelli V, Sinagra G, Zacchigna S, Giacca M. Single-dose intracardiac injection of pro-regenerative microRNAs improves cardiac function after myocardial infarction. *Circ Res*. 2017;120:1298–1304.
37. Pandey R, Velasquez S, Durrani S, Jiang M, Neiman M, Crocker JS, Benoit JB, Rubinstein J, Paul A, Ahmed RP. MicroRNA-1825 induces proliferation of adult cardiomyocytes and promotes cardiac regeneration post ischemic injury. *Am J Transl Res*. 2017;9:3120–3137.
38. Waters R, Alam P, Pacelli S, Chakravarti AR, Ahmed RPH, Paul A. Stem cell-inspired secretome-rich injectable hydrogel to repair injured cardiac tissue. *Acta Biomater*. 2018;69:95–106.
39. Waters R, Pacelli S, Maloney R, Medhi I, Ahmed RP, Paul A. Stem cell secretome-rich nanoclay hydrogel: a dual action therapy for cardiovascular regeneration. *Nanoscale*. 2016;8:7371–7376.
40. Hasan A, Khattab A, Islam MA, Hweij KA, Zeitouny J, Waters R, Sayegh M, Hossain MM, Paul A. Injectable hydrogels for cardiac tissue repair after myocardial infarction. *Adv Sci (Weinh)*. 2015;2:1500122.
41. Soonpaa MH, Kim KK, Pajak L, Franklin M, Field LJ. Cardiomyocyte DNA synthesis and binucleation during murine development. *Am J Physiol*. 1996;271:H2183–H2189.
42. Ortiz-Montero P, Londono-Vallejo A, Vernot JP. Senescence-associated IL-6 and IL-8 cytokines induce a self- and cross-reinforced senescence/inflammatory milieu strengthening tumorigenic capabilities in the MCF-7 breast cancer cell line. *Cell Commun Signal*. 2017;15:17.
43. Sengupta S, Toh SA, Sellers LA, Skepper JN, Koolwijk P, Leung HW, Yeung HW, Wong RN, Sasisekharan R, Fan TP. Modulating angiogenesis: the yin and the yang in ginseng. *Circulation*. 2004;110:1219–1225.
44. Schaal C, Pillai S, Chellappan SP. The Rb-E2F transcriptional regulatory pathway in tumor angiogenesis and metastasis. *Adv Cancer Res*. 2014;121:147–182.
45. Zha Y, Xia Y, Ding J, Choi JH, Yang L, Dong Z, Yan C, Huang S, Ding HF. MEIS2 is essential for neuroblastoma cell survival and proliferation by transcriptional control of M-phase progression. *Cell Death Dis*. 2014;5:e1417.
46. Pacelli S, Acosta F, Chakravarti AR, Samanta SG, Whitlow J, Modaresi S, Ahmed RPH, Rajasingh J, Paul A. Nanodiamond-based injectable hydrogel for sustained growth factor release: preparation, characterization and in vitro analysis. *Acta Biomater*. 2017;58:479–491.
47. Zhou J, Ahmad F, Parikh S, Hoffman NE, Rajan S, Verma VK, Song J, Yuan A, Shanmughapriya S, Guo Y, Gao E, Koch W, Woodgett JR, Madesh M, Kishore R, Lal H, Force T. Loss of adult cardiac myocyte GSK-3 leads to mitotic catastrophe resulting in fatal dilated cardiomyopathy. *Circ Res*. 2016;118:1208–1222.
48. Eppenberger HM, Hertig C, Eppenberger-Eberhardt M. Adult rat cardiomyocytes in culture: a model system to study the plasticity of the differentiated cardiac phenotype at the molecular and cellular levels. *Trends Cardiovasc Med*. 1994;4:187–193.
49. Mahmoud AI, Kocabas F, Muralidhar SA, Kimura W, Koura AS, Thet S, Porrello ER, Sadek HA. Meis1 regulates postnatal cardiomyocyte cell cycle arrest. *Nature*. 2013;497:249–253.
50. Dai Y, Ashraf M, Zuo S, Uemura R, Dai YS, Wang Y, Haider HK, Li T, Xu M. Mobilized bone marrow progenitor cells serve as donors of cytoprotective genes for cardiac repair. *J Mol Cell Cardiol*. 2008;44:607–617.
51. Ahmed RP, Ashraf M, Buccini S, Shujia J, Haider HK. Cardiac tumorigenic potential of induced pluripotent stem cells in an immunocompetent host with myocardial infarction. *Regen Med*. 2011;6:171–178.
52. Nigmatullin R, Bencsik M, Gao F. Influence of polymerisation conditions on the properties of polymer/clay nanocomposite hydrogels. *Soft Matter*. 2014;10:2035–2046.
53. Pacelli S, Paolicelli P, Dreesen I, Kobayashi S, Vitalone A, Casadei MA. Injectable and photocross-linkable gels based on gellan gum methacrylate: a new tool for biomedical application. *Int J Biol Macromol*. 2015;72:1335–1342.
54. Paul A. Nanocomposite hydrogels: an emerging biomimetic platform for myocardial therapy and tissue engineering. *Nanomedicine (Lond)*. 2015;10:1371–1374.
55. Song F, Li X, Wang Q, Liao L, Zhang C. Nanocomposite hydrogels and their applications in drug delivery and tissue engineering. *J Biomed Nanotechnol*. 2015;11:40–52.
56. Li Y, Dong H, Li Y, Shi D. Graphene-based nanovehicles for photodynamic medical therapy. *Int J Nanomedicine*. 2015;10:2451–2459.
57. Paul A, Hasan A, Kindi HA, Gaharwar AK, Rao VT, Nikkhah M, Shin SR, Krafft D, Dokmeci MR, Shum-Tim D, Khademhosseini A. Injectable graphene oxide/hydrogel-based angiogenic gene delivery system for vasculogenesis and cardiac repair. *ACS Nano*. 2014;8:8050–8062.
58. Sokal JE, Shimaoka K. Pyrogen in the urine of febrile patients with Hodgkin's disease. *Nature*. 1967;215:1183–1185.
59. Lee DJ, Cavasin MA, Rocker AJ, Soranno DE, Meng X, Shandas R, Park D. An injectable sulfonated reversible thermal gel for therapeutic angiogenesis to protect cardiac function after a myocardial infarction. *J Biol Eng*. 2019;13:6. eCollection 2019.
60. Mihic A, Cui Z, Wu J, Vlacic G, Miyagi Y, Li SH, Lu S, Sung HW, Weisel RD, Li RK. A conductive polymer hydrogel supports cell electrical signaling and improves cardiac function after implantation into myocardial infarct. *Circulation*. 2015;132:772–784.
61. Hernandez MJ, Christman KL. Designing acellular injectable biomaterial therapeutics for treating myocardial infarction and peripheral artery disease. *JACC Basic Transl Sci*. 2017;2:212–226.

SUPPLEMENTAL MATERIAL

Table S1. Adult rat cardiomyocyte isolation buffer composition.

10X KHB Stock Solution (Total volume= 1L)		**Molarity (mM)**	**Amount (g)**
	NaCl	1180	68.9
	KCl	48	3.5
	HEPES	250	59.7
	$MgSO_4$	12.5	1.4
	K_2HPO_4	12.5	2.1
	Adjust pH to 7.4 with 4M NaOH (~20mL), store at 4°C		

KHB Solution, 500 mL		**Amount**
	10X KHB	50 mL
	Glucose	0.99 g
	Taurine	0.31 g
	Add H_2O to bring volume to 500mL; pH should be ~7.35	

Solution A		**Amount**
	KHB solution	375 mL (10 mM)
	BDM	0.375 g
	Oxygenate with 100% O_2 and warm to 37°C	

Solution B, 50mL		**Amount**
	Solution A	50 mL
	BSA	0.5 g
	0.1 M $CaCl_2$ (Ca^{++}=0.1 mM)	50 µL

Solution E, 50mL		**Amount**
	Solution A	50 mL
	BSA	0.05 g
	Collagenase type II (263 units/mg)	35 mg
	Hyaluronidase (Type I-S)	10 mg
	0.1 M $CaCl_2$ stock	12.5 µL
	Mix well	

$CaCl_2$ Stock, 0.1M		**Amount**
	$CaCl_2$	7.35 g
	H_2O	500 mL
	Then store at 4°C	

Table S2. siRNAs Sequences.

siRNA	**Sequence**
siRb1	CCAGUACCAAAGUUGAUAATT
siMeis2	CCACGAUGAUGCAACCUCATT
Cel-miR-67	UCACAACCUCCUAGAAAGAGUAGA

Table S3. Homology analysis of siRb1 with rat genome.

Discription	Max score	Total score	Query cover	E value	Ident	Accession
Rattus norvegicus retinoblastoma 1 (Rb1), mRNA	38.2	38.2	100%	0.006	100%	NM_017045.1
Rattus norvegicus mRNA for retinoblastoma protein, partial sequence	38.2	38.2	100%	0.006	100%	D25233.1
Rattus norvegicus Y Chr BAC RNECO-131C03 (Amplicon Express Rat SHR-Akr (EcoR1 Digest) BAC library) complete sequence	28.2	78.8	94%	5.4	100%	AC246525.4
Rattus norvegicus BAC CH230-6C14 () complete sequence	28.2	80.8	100%	5.4	100%	AC094946.6
Rattus norvegicus BAC CH230-12M22 () complete sequence	28.2	186	94%	5.4	100%	AC141398.4
Rattus norvegicus 2 BAC CH230-7P18 (Children's Hospital Oakland Research Institute) complete sequence	28.2	80.8	100%	5.4	100%	AC095504.7
Rattus norvegicus Y Chr BAC RNECO-145B11 (Amplicon Express Rat SHR-Akr (EcoR1 Digest) BAC library) complete sequence	28.2	54.5	73%	5.4	100%	AC240959.5
Rattus norvegicus TL0AEA76YE18 mRNA sequence	28.2	28.2	73%	5.4	100%	FQ231233.1
Rattus norvegicus TL0ACA17YL01 mRNA sequence	28.2	28.2	73%	5.4	100%	FQ217794.1
Rattus norvegicus TL0ADA42YK07 mRNA sequence	28.2	28.2	73%	5.4	100%	FQ220503.1

Homology analysis of siRb1 with rat genome: Table represents the significance base top 10 homology results, which demonstrates the specific and 100% identity of siRb1 with rat Rb1 gene with a significant *p*-value (p=0.002).

Table S4. Homology analysis of siMeis2 with rat genome.

Description	Max score	Total score	Query cover	E value	Ident	Accession
PREDICTED: Rattus norvegicus Meis homeobox 2 (Meis2), transcript variant X13, mRNA	38.2	38.2	100%	0.007	100%	XM_006234755.3
PREDICTED: Rattus norvegicus Meis homeobox 2 (Meis2), transcript variant X12, mRNA	38.2	38.2	100%	0.007	100%	XM_006234754.3
PREDICTED: Rattus norvegicus Meis homeobox 2 (Meis2), transcript variant X11, mRNA	38.2	38.2	100%	0.007	100%	XM_006234753.3
PREDICTED: Rattus norvegicus Meis homeobox 2 (Meis2), transcript variant X10, mRNA	38.2	38.2	100%	0.007	100%	XM_006234752.3
PREDICTED: Rattus norvegicus Meis homeobox 2 (Meis2), transcript variant X9, mRNA	38.2	38.2	100%	0.007	100%	XM_006234751.3
PREDICTED: Rattus norvegicus Meis homeobox 2 (Meis2), transcript variant X8, mRNA	38.2	38.2	100%	0.007	100%	XM_006234750.3
PREDICTED: Rattus norvegicus Meis homeobox 2 (Meis2), transcript variant X7, mRNA	38.2	38.2	100%	0.007	100%	XM_006234749.3
PREDICTED: Rattus norvegicus Meis homeobox 2 (Meis2), transcript variant X6, mRNA	38.2	38.2	100%	0.007	100%	XM_006234748.3
PREDICTED: Rattus norvegicus Meis homeobox 2 (Meis2), transcript variant X5, mRNA	38.2	38.2	100%	0.007	100%	XM_006234747.3

PREDICTED: Rattus norvegicus Meis homeobox 2 (Meis2), transcript variant X4, mRNA	**38.2**	**38.2**	**100%**	**0.007**	**100%**	**XM_006234746.3**
PREDICTED: Rattus norvegicus Meis homeobox 2 (Meis2), transcript variant X3, mRNA	**38.2**	**38.2**	**100%**	**0.007**	**100%**	**XM_006234745.3**
PREDICTED: Rattus norvegicus Meis homeobox 2 (Meis2), transcript variant X2, mRNA	**38.2**	**38.2**	**100%**	**0.007**	**100%**	**XM_006234744.3**
PREDICTED: Rattus norvegicus Meis homeobox 2 (Meis2), transcript variant X1, mRNA	**38.2**	**38.2**	**100%**	**0.007**	**100%**	**XM_006234743.3**
Rattus norvegicus Meis homeobox 2 (Meis2), mRNA	**38.2**	**38.2**	**100%**	**0.007**	**100%**	**NM_001107758.1**
Rattus norvegicus serine/arginine repetitive matrix 2 (Srrm2), mRNA	**28.2**	**28.2**	**73%**	**7.1**	**100%**	**NM_001277154.1**
PREDICTED: Rattus norvegicus cytidine monophospho-N-acetylneuraminic acid hydroxylase (Cmah), transcript variant X7, mRNA	**26.3**	**26.3**	**68%**	**28**	**100%**	**XM_017600609.1**
PREDICTED: Rattus norvegicus cytidine monophospho-N-acetylneuraminic acid hydroxylase (Cmah), transcript variant X6, misc_RNA	**26.3**	**26.3**	**68%**	**28**	**100%**	**XR_001841737.1**

Homology analysis of siMeis2 with rat genome: Table represents the significance base top 17 homology results, which demonstrates the specific and 100% query coverage of siMeis2 with rat Meis2 gene (variants) with a significant *p*-value (*p*=0.002).

Table S5. List of antibodies used in the study.

	Antibody	Catalog #	Company
1	Rabbit anti-β-actin	A1978	Sigma-Aldrich
2	Rabbit anti-GAPDH	G9545	Sigma-Aldrich
3	Rabbit anti-aurora B	A5102	Sigma-Aldrich
4	Mouse anti- cardiac troponin-T	MA5-12960	Thermo Scientific
5	Rabbit-anti-Rb1	10048-2-Ig	Proteintech
6	Rabbit anti-cardiac troponin-I	sc-15368	Santa Cruz Biotechnology
7	Goat-anti-Meis1/2	Sc-10599	Santa Cruz Biotechnology
8	Rabbit anti-VEGF	sc-152	Santa Cruz Biotechnology
9	Rabbit-anti-Bax	2772S	Cell Signaling Technology
10	Rabbit anti-β-catenin	9562S	Cell Signaling Technology
11	Rabbit anti-p16	ab51243	Abcam
12	Mouse-anti-Histone H3	Ab6002	Abcam
13	Mouse anti-Ki67	550609	BD Pharmingen
14	ECL anti-mouse-HRP	NA931V	GE Healthcare
15	ECL anti-rabbit-HRP	NA9340V	GE Healthcare
16	Goat anti-mouse Alexa fluor 488	A11029	Life Technologies
17	Goat anti-mouse Alexa fluor 594	A11005	Life Technologies
18	Goat anti-rabbit Alexa fluor 488	A11008	Life Technologies
19	Goat anti-rabbit Alexa fluor 594	A11037	Life Technologies

Table S6. RT PCR primer sequences.

RT PCR primers		
Gene		**5’ to 3’**
Rb1	Forward	GTCTGCCAACACCCACAAAA
Rb1	Reverse	ATCCTTCGATGTCAAAGCGC
Meis2	Forward	TGATAACTTCTGCCACCGGT
Meis2	Reverse	GGTTGCATCATCGTGGTCTC
Aurora B	Forward	CAGGGAGAGCTGAAGATTGC
Aurora B	Reverse	ACTGTGGCTAGGGCTCTCAA
Cyclin D1	Forward	CCTGGACCGTTTCTTGTCTC
Cyclin D1	Reverse	CCATTTGAGCTTGTTCACCA
E2F2	Forward	GGCAGACAGTCCTACCAAGG
E2F2	Reverse	CAAGGGGACAAGGGATGGTG
E2F3	Forward	CGAGAGTGGCCATCAGTACC
E2F3	Reverse	ACTTCTTGGTGAGCAGACCG
VEGF	Forward	CTCTCTCCGGAGTAGCCGT
VEGF	Reverse	CTCCTCTCCCTTCTGGAACC
IL6	Forward	CCACTGCCTTCCCTACTTCA
IL6	Reverse	TCTGACAGTGCATCATCGCT
β-actin	Forward	ACCCTAAGGCCAACCGTGAAA
β-actin	Reverse	GTACGACCAGAGGCATACAGG

Figure S1. *In vitro* ACM survivability in culture.

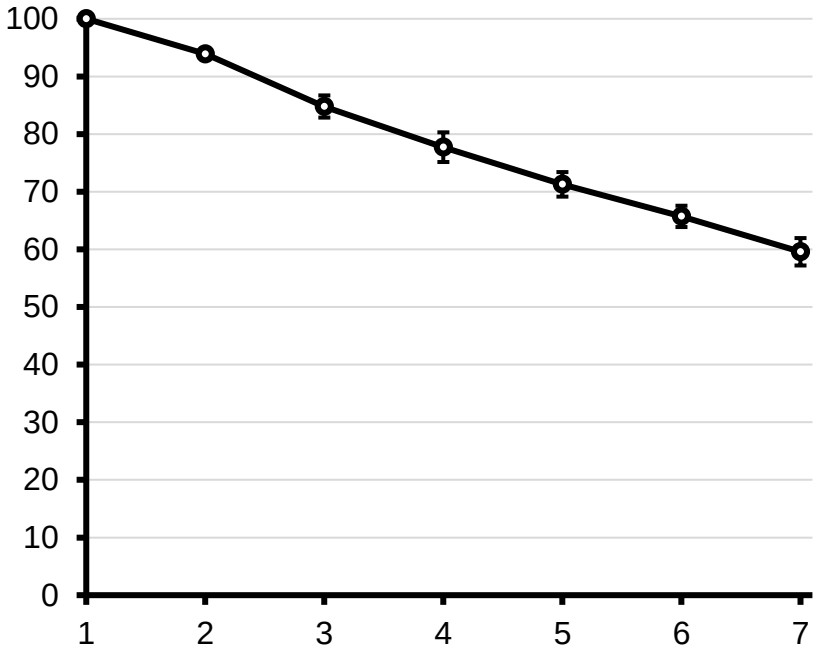

A day wise analysis demonstrates the 59.58±2.38% ACM survival on day 7 after the Lipofectamine 2000 treatment. N= 3 rats, n= 6 experimental replicates each.

Figure S2. Transfection efficacy.

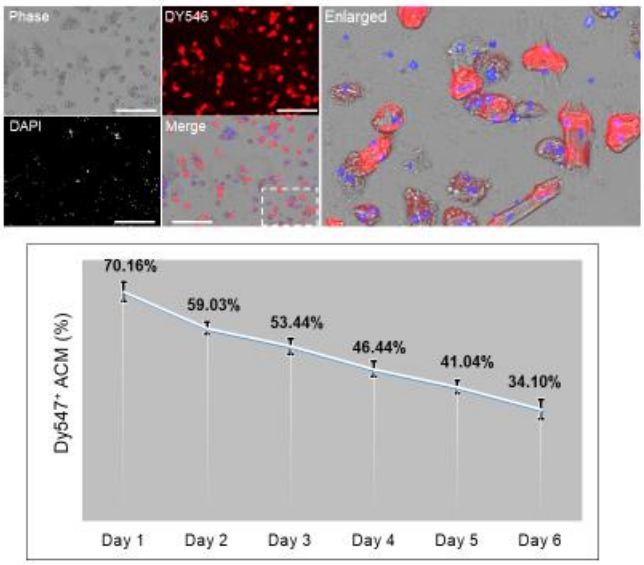

Representative immunostaining images following Dy546 labeled siRNA-cel-67 transfection of ACM. 69.12% of ACMs were positive for Dy546-siR-cel-67 at 24hrs following transfection, whereas, 34.10% ACM were positive for Dy546-siR-cel-67 on day 7. Panels in white rectangles represent respective enlarged sections. Bar graph represents the percent of ACM, transfected with Dy546-siR-cel-67. N= 3 rats, n= 4 experimental replicates each, and n= 3 images each. DAPI= 4′,6-diamidino-2-phenylindole. Scale bar=200 μm.

Figure S3. Transfection efficacy following siUbc transfection.

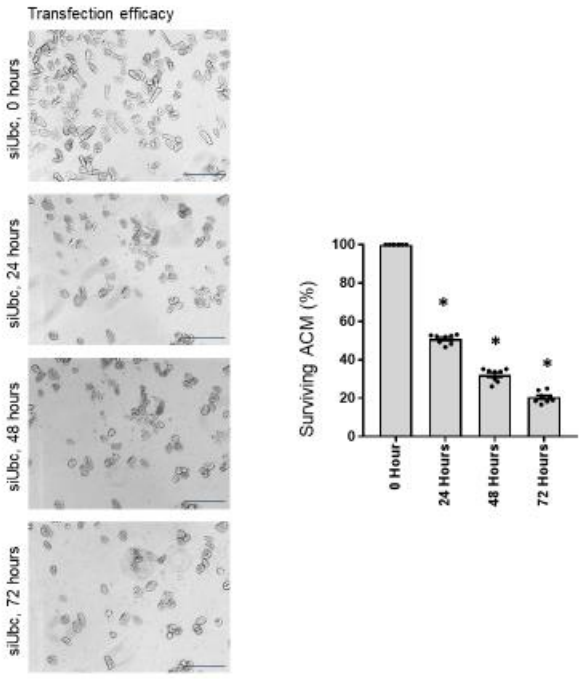

Representative bright field images at different time points for siUbc transfection of ACMs. Bar graph represents the percent of live ACM, after siUbc transfection at different time points. Only 20% ACMs survive at 72hrs post siUbc transfection. *= *p*-value ≤0.05. *P* value ≤0.05 was considered statistically significant. N= 6 rats, n= 8 experimental replicates each, and n= 10 images each. Scale bar=200 μm.

Figure S4. Simultaneous inhibition of *Rb1* and *Meis2* is necessary for ACM proliferation.

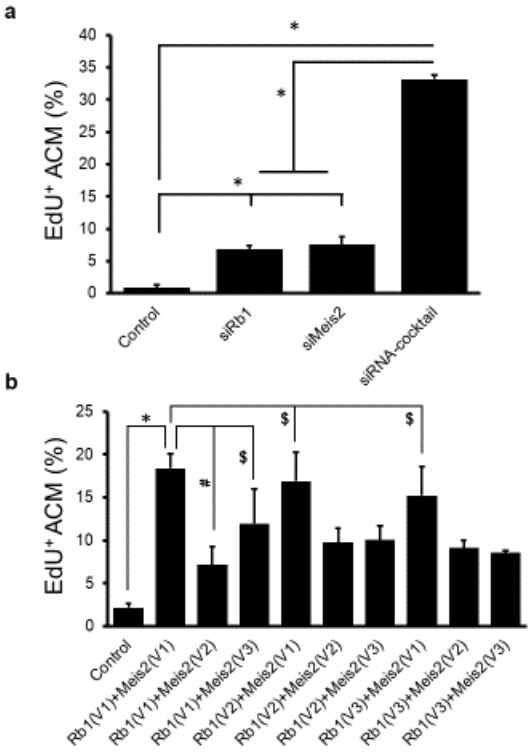

(a) Quantification of DNA synthesis marker, EdU incorporated ACMs on Day 6 after siRNA transfection as depicted. siRNA-cocktail transfection shows superior induction of ACM proliferation compared to the individual Rb1 or Meis2 knockdown approach. (b) Quantification of EdU incorporated ACMs transfected with all combinations of three independent sets of siRNAs against each Rb1 and Meis2. Rb1(V1)+Meis2(V1) is referred to as “siRNA-cocktail” in this manuscript gave the highest amount of induced ACM proliferation. All the experiments were performed using ACM, isolated from rats (~12 weeks old). N= 3 rats, n= 6 experimental replicates each. EdU= 5-ethynyl-2'-deoxyuridine, V= version. *=*p* value ≤0.05; #= *p* value=0.054; $=*p* value >0.05.

Figure S5. Nucleation analysis of ACM.

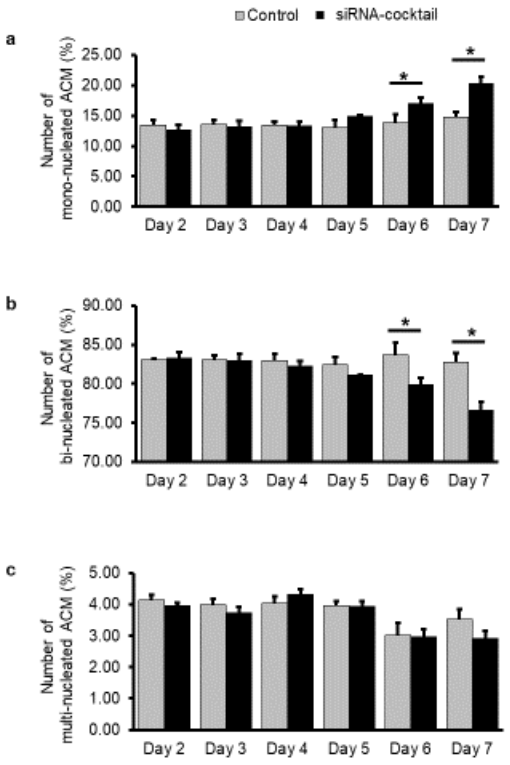

Time course nucleation analysis reveals the state of nuclei in ACM during the course of experiments. It further demonstrates (a) significant increase in number of mono-nuclear ACM, and (b) significant decrease in number of bi-nucleated ACM in siRNA-cocktail transfected group on and after day 6 when compared to control, whereas we did not find any difference in number of multi-nucleated ACM between siRb1+siMeis2 transfected group and control (c). N= 3 rats and n= 8 experimental replicates. *= *p*-value ≤0.05. *P* value ≤0.05 was considered statistically significant.

Figure S6. Time course of ACM proliferation upon simultaneous inhibition of *Rb1* and *Meis2*.

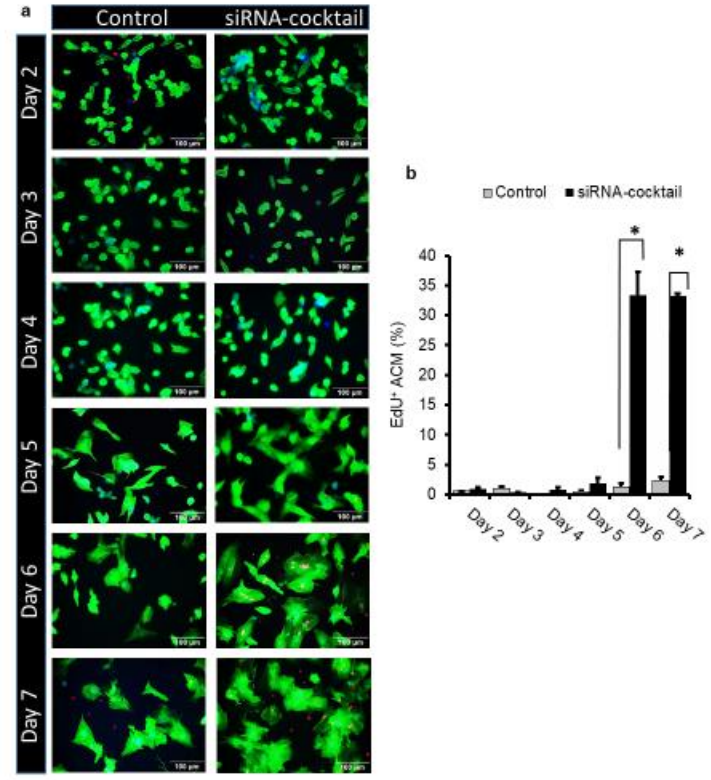

(a,b) Immunostaining shows induction of ACM proliferation on Day 6 after siRNA-cocktail transfection. ACMs were marked by Troponin (green), DNA synthesis was marked by EdU (red), whereas, nuclei were marked by DAPI (blue). All the experiments were performed using ACM, isolated from rats (~12 weeks old). N= 3 rats, n= 8 experimental replicates each, and n= 10 images each. Scale bar=100 µm. EdU= 5-ethynyl-2'-deoxyuridine. *= *p*-value ≤0.05. *P* value ≤0.05 was considered statistically significant.

Figure S7. Simultaneous inhibition of *Rb1* and *Meis2* leads to ACM cell cycle progression.

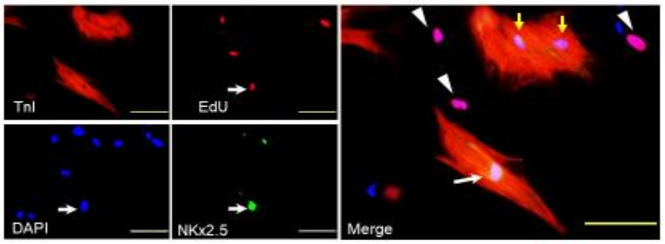

Immunostaining shows co-localization of cardiac-specific nuclear marker Nkx2.5 and EdU in ACM in the siRNA-cocktail treated group. 26.05±1.28% of ACM were positive for both, EdU as well as Nkx2.5 in siRNA-cocktail transfected groups. White arrows indicate the co-localization of EdU with Nkx2.5 in mono-nucleated ACM. Yellow arrows indicate the ACM with Nkx2.5 without EdU. Arrowheads are indicating the EdU positive noncardiomyocytes, which are not showing the Nkx2.5. N= 3 rats and n= 5 experimental replicates each. TnI= Troponin I, EdU= 5-ethynyl-2'-deoxyuridine, DAPI= 4′,6-diamidino-2-phenylindole, NKx2.5= NK2 Homeobox 5. Scale bar=100 µm.

Figure S8. Simultaneous inhibition of *Rb1* and *Meis2* leads to ACM mitosis.

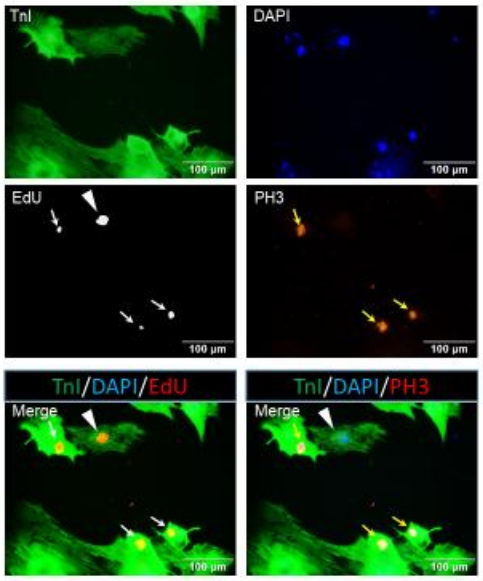

Immunostaining shows co-localization of mitosis marker (PH3; red) and DNA synthesis marker (EdU; far red) in TnI labeled ACMs from the siRNA-cocktail transfected groups. Arrows indicate the co-localization of Edu and PH3 in mono-nucleated ACM, whereas, the arrowhead indicates the bi-nucleated ACM, which shows EdU but not the PH3. N= 3 rats and n= 6 experimental replicates each. TnI= Troponin I, EdU= 5-ethynyl-2'-deoxyuridine, DAPI= 4′,6-diamidino-2-phenylindole, PH3= phosphor histone 3. Scale bar=100 µm.

Figure S9. Simultaneous inhibition of *Rb1* and *Meis2* improves ACM survivability.

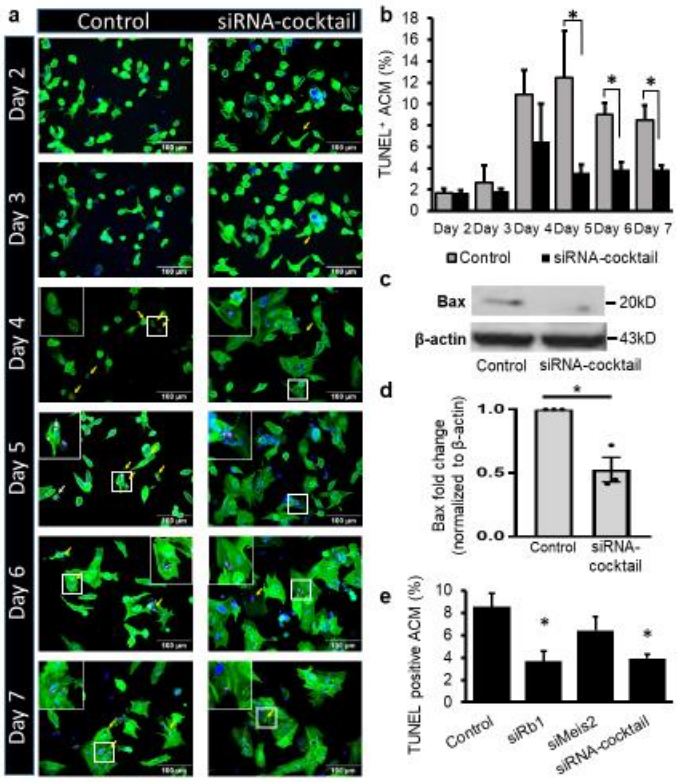

(a,b) Immunostaining shows a significantly lower TUNEL positive ACMs after day 3 in the siRNA-cocktail transfected group when compared to control. ACMs were marked by Troponin (green), cell survivability was analyzed through TUNEL assay (red), whereas, nuclei were marked by DAPI (blue). Arrows indicate the TUNEL^{+} ACMs. Panels in white rectangles represent respective enlarged sections. (c) Immunoblot for apoptotic marker Bax from the cell lysate of ACMs, per depicted groups. (d) The densitometric analysis shows a significant downregulation in Bax expression in the siRNA-cocktail transfected group compared to control. (e) TUNEL assay for Individual Rb1 or Meis2 knockdowns compared to siRNA-cocktail. All the experiments were performed in triplicate using ACMs, isolated from rat (~12 weeks old). N= 3 rats, n= 3 experimental replicates each, and n= 10 images each. TnI= Troponin I, TUNEL= Terminal deoxynucleotidyl transferase dUTP nick end labeling, DAPI= 4′,6-diamidino-2-phenylindole. Scale bar=100 μm *= *p*-value ≤0.05. *P* value ≤0.05 was considered statistically significant.

Figure S10. Expression analysis of cell cycle associated genes in ACMs after simultaneous inhibition of *Rb1* and *Meis2*.

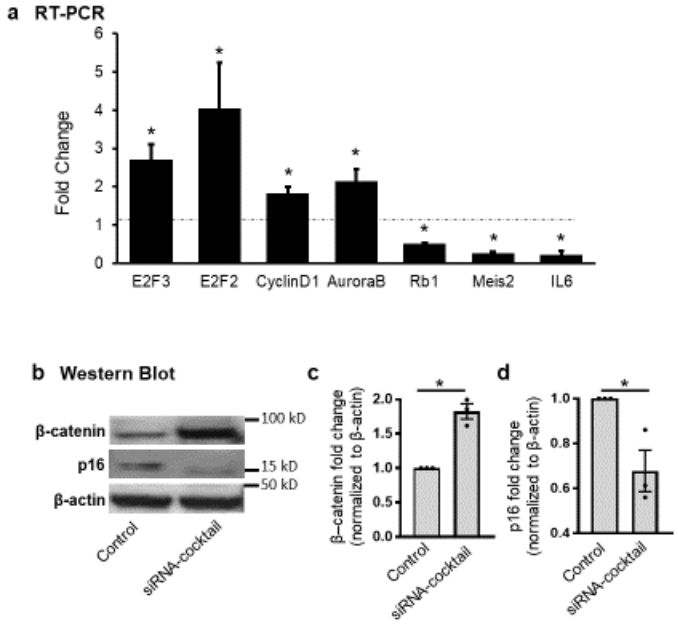

(a) RT-PCR expression analysis is showing a significant increase in the expression of E2F2, E2F3, Cyclin D1, and Aurora B; whereas, *Rb1*, *Meis2*, and IL6 are down-regulated in the siRNA-cocktail transfected group when compared to control. (b) Representative immunoblots for β-catenin and p16 expression. Immunoblotting was performed with cell lysate from ACMs, transfected with siRNA-cocktail and control. (c,d) Densitometric analysis showed regulation in the expression of cell cycle regulators in the siRNA-cocktail transfected group in comparison to control. All the experiments were performed in triplicate using ACMs, isolated from adult rats (~12 weeks old). N= 3 rats, n= 3 experimental replicates each, and n= 10 images each. Results are presented as mean±SEM; * = *p*-value ≤0.05. *P* value ≤0.05 was considered statistically significant.

Figure S11. Improved ACMs survivability after hydrogel mediated delivery of *siRb1* and *siMeis2* in adult animals post-MI.

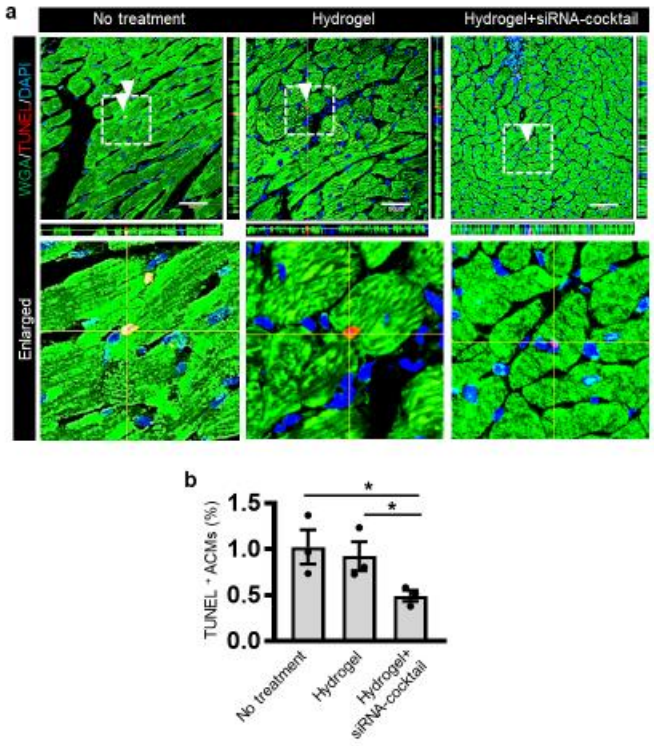

(a,b) Immunostaining images are showing a significant decrease in TUNEL positive ACMs in the siRNA-cocktail treated group versus controls. Panels in yellow rectangles represent respective enlarged sections. N= 4 rats per group, n= 5 non-serial sections were imaged each, and n= 5 separate regions quantified each. Scale bar=50 μm. WGA= Wheat germ agglutinin, TUNEL= Terminal deoxynucleotidyl transferase dUTP nick end labeling, DAPI= 4′,6-diamidino-2-phenylindole. Results are presented as mean±SEM; * = *p*-value ≤0.05. *P* value ≤0.05 was considered statistically significant.

Figure S12. Expression of cell cycle associated genes after hydrogel mediated delivery of *siRb1* and *siMeis2* in adult animals post-MI.

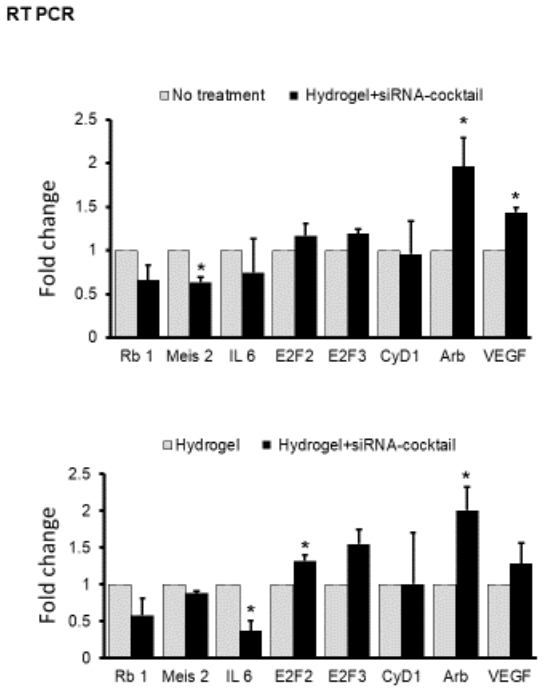

(a,b) RT-PCR analysis shows an increased expression of *E2F2, E2F3, Aurora B,* and *VEGF*; whereas, *Rb1*, *Meis2*, and *IL6* are down-regulated in the siRNA-cocktail group compared to controls. RT-PCR was performed with total RNA isolated from heart tissues of adult rats from different groups (~12 weeks old). N= 4 rats per group and n= 6 experimental replicates each. Expression analysis was performed on day 21 after MI. Results are presented as mean±SEM; * = *p*-value ≤0.05. *P* value ≤0.05 was considered statistically significant.

Figure S13. Western blot analysis of cell cycle associated genes after hydrogel mediated delivery of siRb1 and siMeis2 in adult animals post-MI.

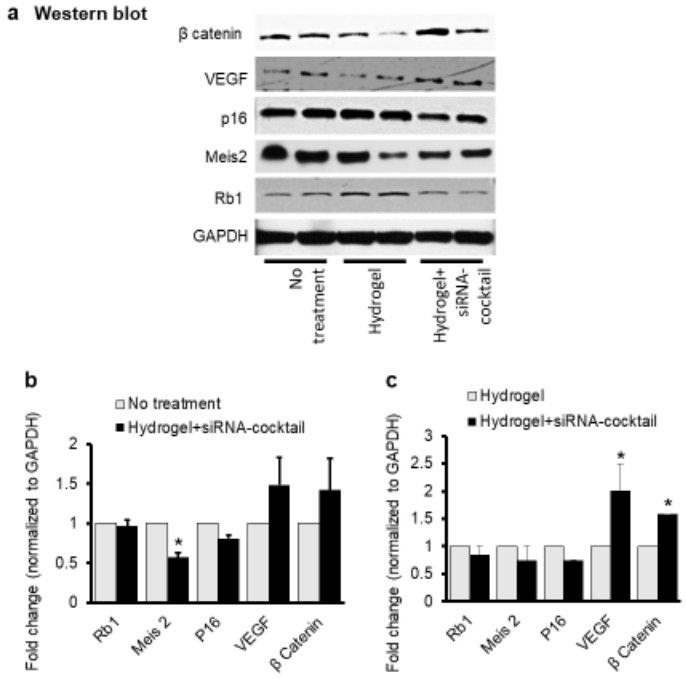

(a) Representative immunoblots for Rb1, Meis2, p16, and VEGF. Immunoblotting was performed using tissue lysates, from heart tissues of adult rats from different groups (~12 weeks old, N= 4 rats per group, and n= 3 experimental replicates each). (b,c) Densitometry analysis showed differential expression of proteins among the three groups. N= 3 rats per group and n= 3 experimental replicates each. Expression analysis was performed on day 21 after MI. Results are presented as mean±SEM; * = *p*-value ≤0.05. *P* value ≤0.05 was considered statistically significant.

Figure S14. Effects of *siRb1* and *siMeis2* knockdown on Endothelial and Fibroblast cells.

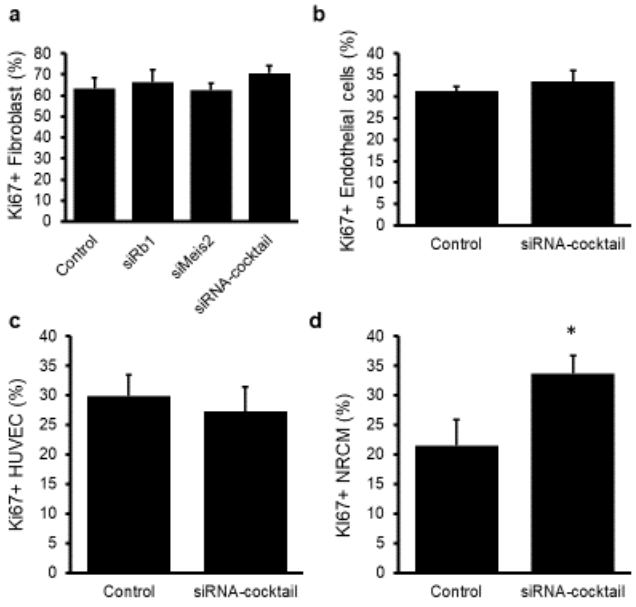

(a) Quantification of antibody labeling against a cellular marker for proliferation, Ki67, within cardiac fibroblasts showing no difference of increased proliferation on Day 6 after siRNA transfection as depicted. (b,c) Similar results were obtained when using either isolated cardiac endothelial cells (b) or HUVEC cells (c). (d) siRNA-cocktail transfection of NRCMs results in an enhancement of endogenous proliferation rate, showing a selective effect of Rb1 and Meis2 on the control of ACM senescence. N= 6 rats, n= 8 experimental replicates each. HUVEC= Human Umbilical Vein Endothelial Cells. *= p-value ≤0.05.

Figure S15. Cardiac function analysis at baseline with hydrogel injection.

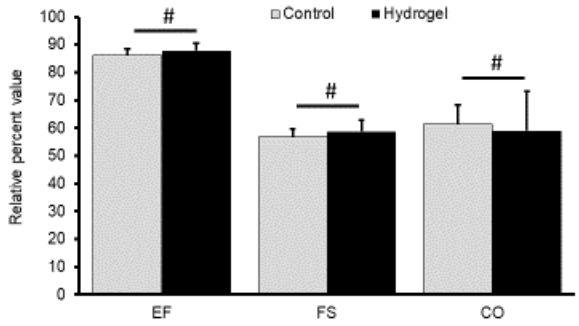

Bar graph shows no significant difference in ejection fraction, fractional shortening, and cardiac output between the hydrogel alone intramyocardial injected group and the PBS injected control group at day 21. N= 6 rats per group. EF= ejection fraction, FS= fractional shortening, CO= and cardiac output. #= *p*-value ≥0.05. *P* value ≤0.05 was considered statistically significant. EF; ejection fraction: FS; fractional shortening: CO; and cardiac output.

Figure S16. Cardiac function analysis with strain echocardiography after injury.

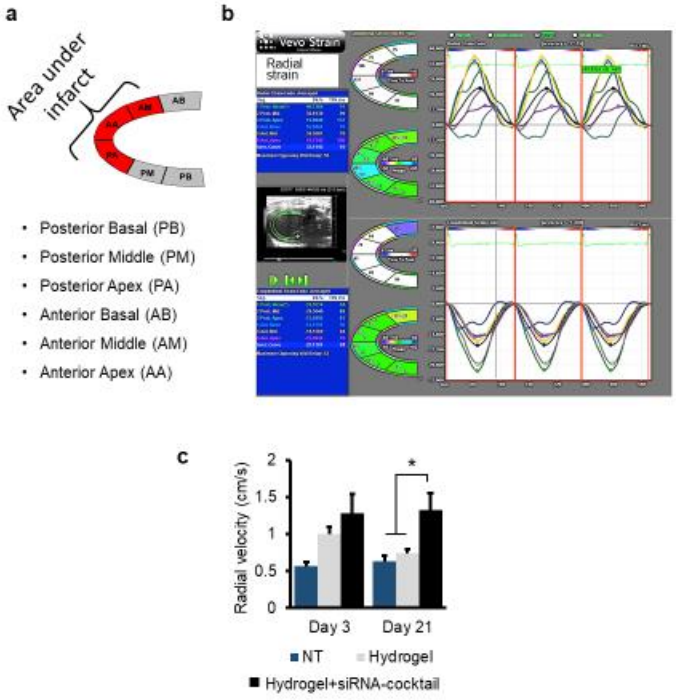

(a) A schematics overview of six segments of the myocardial wall, highlighting the segments, anticipated to be at the infarcted area. **(b)** Representative echocardiographic image for radial and longitudinal strain after MI in hydrogel-siRNA-cocktail treated groups. **(c)** The bar graph shows a significantly improved Radial velocity in hydrogel-siRNA-cocktail treated groups *versus* controls at day 21 post-MI. N= 6 rats per group. NT= no treatment. *= *p*-value ≤0.05. *P* value ≤0.05 was considered statistically significant.

Figure S17. Real-time imaging of proliferating ACMs after *Rb1* and *Meis2* knockdown.

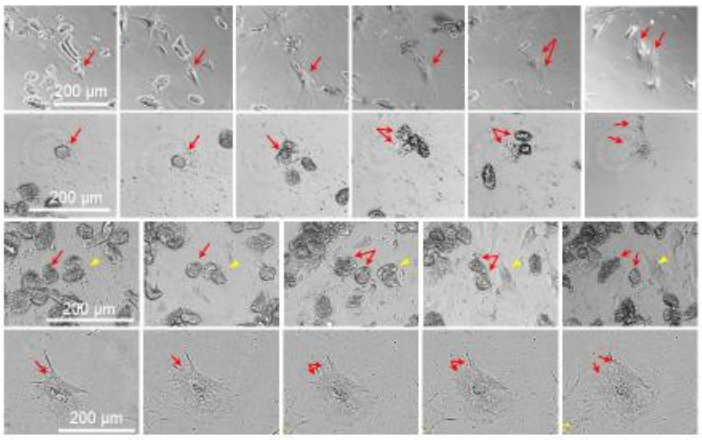

Bright field images captured with live cell imaging with Incucyte® Live Cell Analysis System. Each row shows a cytokinesis event captured between days 3 and 6 post siRNA-cocktail transfection. Red arrows are showing the appearance of dividing ACMs. Yellow arrowheads are pointing at a non-dividing cell. N= 3 rats, n= 8 experimental replicates each (~12 weeks old). Scale bars=200 µm.

Figure S18. Homology analysis of siRb1 with rat genome.

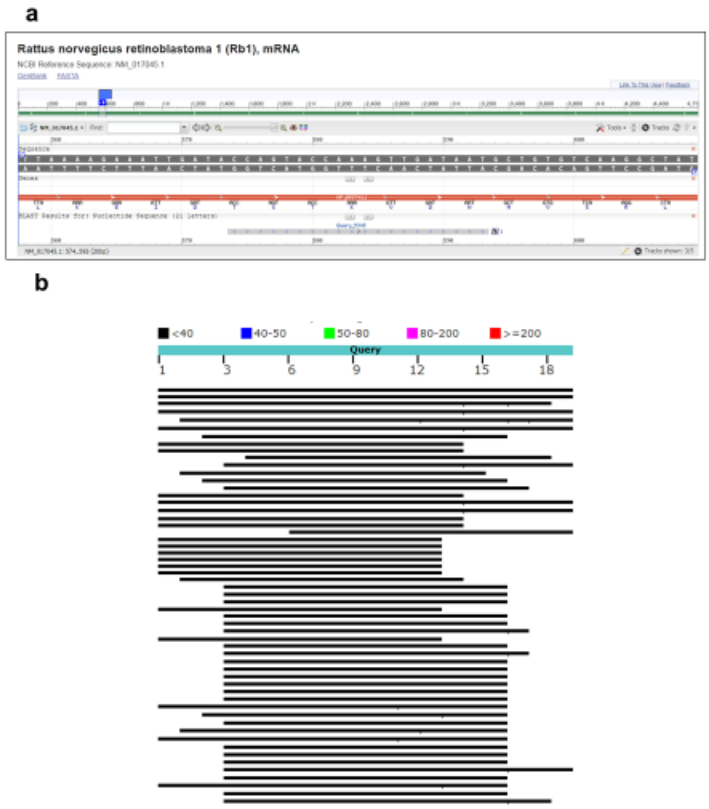

(a) Homology alignment for siRb1 with rat genome (b) demonstrate the specific binding of siRNA with rat Rb1 gene.

Figure S19. Homology analysis of siMeis2 with rat genome.

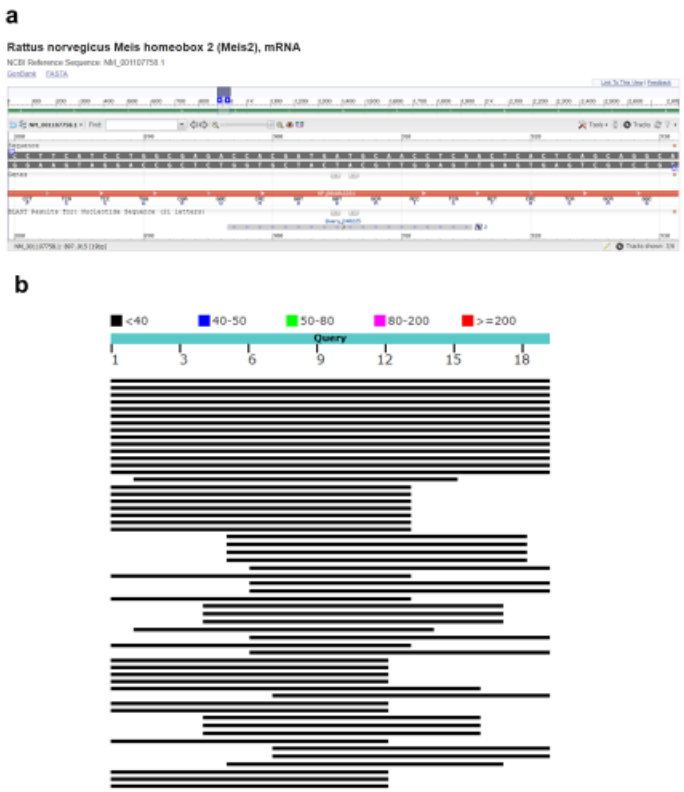

(a) Homology alignment for siMeis2 with rat genome (b) demonstrate the specific binding of siRNA with rat Meis2 gene.

Supplemental Video Legend:

Video S1. Live cell video of a beating ACM on day 7. ACMs retain their physiological characteristics up until day 7, as shown by beating ACM. N= 3 rats. Best viewed with Windows Media Player.